

Dark phase transition from WIMP: complementary tests from gravitational waves and colliders

Shinya Kanemura^a and Shao-Ping Li^b

^a*Department of Physics, Osaka University, Toyonaka, Osaka 560-0043, Japan*

^b*Institute of High Energy Physics, Chinese Academy of Sciences, Beijing 100049, China*

E-mail: kanemu@het.phys.sci.osaka-u.ac.jp, spli@ihep.ac.cn

ABSTRACT: A dark sector is an interesting place where a strong first-order phase transition, observable gravitational waves and/or a dark matter candidate could arise. However, the experimental tests for such a dark sector could be ambiguous due to the dark content, largely unconstrained parameter space and the connection to the visible world. We consider a minimal dark scalar-vector boson plasma to realize the three mentioned phenomena, with a unique connection to the Standard Model via the Higgs portal coupling. We discuss the important features of the Higgs portal in such a minimal dark sector, namely the dark thermalization, collider tests, and direct detection of dark matter. We perform numerical analyses of the dark phase transition associated with stochastic gravitational waves and dark matter, discussing the complementarity of collider detection, dark matter direct detection and space-based/terrestrial interferometers as a promising avenue to hear and see the minimal dark sector.

Contents

1	Introduction	1
2	A minimal Higgs-portal dark $U(1)_X$ with DM	3
2.1	Theoretical framework	3
2.2	Higgs portal for dark mediator detection	4
2.3	Higgs portal for dark thermalization	5
3	Dark gauge boson as WIMP-like DM	8
3.1	Relic density	8
3.2	Higgs portal for DM direct detection	10
3.3	Higgs portal for DM indirect detection	11
4	Dark phase transition from a minimal hot boson plasma	12
4.1	Effective potential	12
4.2	Dynamics of dark phase transition	14
5	GW profiles	15
6	Hear and see the dark: complementary tests of DM, GW and colliders	19
7	Conclusion	21
A	An analytic perspective of the minimal dark phase transition	22
B	DM annihilation rates	24

1 Introduction

An Abelian dark gauge sector is one of the simplest scenarios that could undergo a strong first-order phase transition in the early universe and produce observable gravitational waves (GW) [1]. The dark sector is also a natural place for the dark matter (DM) candidate which annihilates into dark species in a weakly-interacting-massive-particle (WIMP) like pattern [2–5]. The dark sector could also be detectable at colliders, depending on the portal couplings to the Standard Model (SM) [6, 7].

A strong first-order phase transition in a dark Abelian gauge sector was widely considered via a scale-invariant scalar potential [8–16] or a scale-breaking one [17–22]. Moreover, the interesting connection among the phase transition, GW and DM has received increased attention [14, 23–33], where complementary tests from DM detection and GW interferometers can be a promising avenue to probe the dark sector. In this respect, the hidden world

becomes not so *dark* as its name suggests, since we will be able to not only hear but also see the dark.

In this paper, we consider a dark gauge $U(1)_X$ sector to realize a strong first-order phase transition, GW signals and a stable DM candidate. The results presented in this paper will differ from previous work in several aspects. First of all, unlike a scale-invariant dark sector with a radiative symmetry breaking [34], we consider a dark phase transition with a vacuum mass term, so that the $U(1)_X$ symmetry breaking occurs spontaneously via the Higgs-like mechanism. On the other hand, we take a minimal perspective to consider a scale-breaking dark sector such that it only consists of a dark scalar and a dark gauge boson (a boson plasma). Without any fermionic DM, the dark gauge boson carrying an unbroken Z_2 symmetry can itself play the role of a WIMP-like DM candidate. Besides, the dark phase transition is dominantly triggered by the finite-temperature correction from the DM, therefore allowing one to obtain stronger connection among the dark phase transition, GW and DM, and in particular for the complementary probes.

In addition to the minimal setup of the dark boson plasma, we further discuss the important role of the Higgs portal coupling, which is the unique renormalizable connection between the dark boson plasma and the SM sector due to the unbroken Z_2 symmetry. We will specify three significant features of the Higgs portal for the minimal dark boson plasma, including the dark thermalization, collider detection and DM direct detection.

Dark thermalization has been noticed in a hidden phase transition, and it was found that if the dark sector is colder than the SM plasma [19], the induced GW signals could be suppressed by a factor of $\xi^8 (\ll 1)$ [22], where ξ is the temperature ratio of the dark and the SM sectors. Therefore, the Higgs portal coupling is essential to induce strong GW signals from the one-temperature ($\xi = 1$) dark phase transition. The Higgs portal also opens up collider detection of the dark scalar, which acts as the mediator between the two sectors. In particular, direct production of a heavy dark scalar at the upcoming/proposed high-luminosity (HL) LHC [35], Compact Linear Collider (CLIC) [36], International Linear Collider (ILC) [37], and muon colliders [38] could serve as the collider tests for the dark sector. Moreover, direct detection of the gauge boson DM is also possible via a proper range of the Higgs portal which explains the null observation of the existing DM direct detection from LUX [39], XENON1T [40], PandaX-II [41], PandaX-4T [42] and LUX-ZEPLIN (LZ) [43] experiments.

We will present several benchmark points (BP) that can induce observable GW signals by space-based interferometers, including LISA [44], BBO [45], and DECIGO [46], and by some atomic interferometers, such as the km-scale terrestrial experiment AION [47] and the strontium atomic interferometer AEDGE [48]. We further scrutinize each BP to seek for complementary tests from colliders and DM direct detection in, e.g., the LZ experiment [49–51] above the neutrino floor [52, 53].

The paper is outlined as follows. In Sec. 2, we present the minimal dark $U(1)$ framework and discuss the Higgs portal interaction as the window for collider tests as well as for the dark thermalization. In Sec. 3, we calculate the DM relic density and discuss the DM direct detection via the Higgs portal. Then in Sec. 4, we perform a numerical analysis of the dark phase transition, and Sec. 5 is devoted to the discussion of GW profiles relevant for the dark

phase transition. Complementary tests of colliders, DM and GW from the minimal dark boson plasma are shown in Sec. 6. Finally, conclusions are made in Sec. 7. An analytic derivation of the dark phase transition is presented in Appendix A to efficiently show the favored parameter space, and the calculation of the DM annihilation rate is relegated to Appendix B.

2 A minimal Higgs-portal dark $U(1)_X$ with DM

2.1 Theoretical framework

The minimal dark gauge $U(1)_X$ sector contains only two bosons, the dark scalar and the dark gauge boson. Here, we consider a generic scalar potential without classical scale invariance. The tree-level scalar potential in vacuum is written as

$$V_0(S) = -\mu_S^2 |S|^2 + \lambda |S|^4, \quad (2.1)$$

where $\mu_S^2 > 0$ and $S = (v_\phi + \phi + i\chi)/\sqrt{2}$ is the dark scalar singlet charged under $U(1)_X$ with v_ϕ the vacuum expectation value (VEV). ϕ is the dark scalar and χ the Goldstone boson associated with the gauge $U(1)_X$ symmetry breaking.

The dark boson plasma can exhibit Z_2 -parity conservation, in which the scalar and gauge boson transform as [54, 55]

$$A'_\mu \rightarrow -A'_\mu, \quad S \rightarrow S^*. \quad (2.2)$$

The Z_2 symmetry forbids the kinetic mixing $B'_{\mu\nu} B^{\mu\nu}$, where $B'_{\mu\nu} = \partial_\mu A'_\nu - \partial_\nu A'_\mu$ and $B_{\mu\nu} = \partial_\mu B_\nu - \partial_\nu B_\mu$ with B_μ the Abelian gauge fields in the SM sector. After the gauge $U(1)_X$ symmetry breaking, the Z_2 symmetry is retained, so that the dark gauge boson becomes a stable DM candidate. It should be mentioned that, however, both the dark scalar and the dark gauge boson can be long-lived DM without the Z_2 parity, provided that they are lighter than ~ 1 MeV and the Higgs portal coupling as well as the kinetic mixing is sufficiently small. Nevertheless, when all the renormalizable portal couplings between the SM and the dark sectors are sufficiently small, it becomes much more difficult to probe the dark in collider experiments.

After the gauge $U(1)_X$ symmetry breaking, the gauge boson DM acquires mass via the dark vacuum v_ϕ . Without fermions, there is freedom to normalize the gauge charge of the dark scalar such that,

$$m_{A'} = g_X v_\phi, \quad (2.3)$$

where g_X denotes the dark gauge coupling. Since v_ϕ, g_X are relevant for the phase transition and GW, while the DM relic density and direct detection depend on g_X and $m_{A'}$, we expect that there exists some correlation among the dark phase transition, the induced GW signals and the DM phenomenology, which we are about to investigate in this paper.

2.2 Higgs portal for dark mediator detection

In the presence of an unbroken Z_2 parity, the only renormalizable interaction between the minimal dark and SM sectors comes from the Higgs portal coupling,

$$\mathcal{L} \supset \lambda_p |S|^2 |H|^2, \quad (2.4)$$

where $H = (0, (v_{\text{EW}} + h)/\sqrt{2})^T$ is the SM Higgs doublet with $v_{\text{EW}} = 246$ GeV the electroweak VEV. While the portal interaction may assist in the electroweak phase transition, an $\mathcal{O}(1)$ λ_p is generically required [56–58]. Since we are concerned with a dark phase transition, we assume a small portal coupling such that it has a negligible impact on the electroweak and dark phase transitions. With a small λ_p , the tree-level minimization condition from potential (2.1) approximately gives rise to

$$\mu_S^2 \approx \lambda v_\phi^2, \quad m_\phi^2 \approx 2\lambda v_\phi^2, \quad (2.5)$$

where m_ϕ is the physical mass of the dark scalar¹.

The Higgs portal coupling can play three important roles in the minimal dark sector, as we shall discuss in subsequent sections. First of all, the scalar-Higgs mixing after gauge symmetry breaking can induce couplings between the dark scalar and the SM particles. For instance, the effective coupling between ϕ and the SM fermions is given by $\theta m_f/v_{\text{EW}}$, with m_f the fermion mass and θ the scalar-Higgs mixing angle given by

$$\theta \approx \frac{v_{\text{EW}} v_\phi \lambda_p}{m_h^2 - m_\phi^2}, \quad (2.6)$$

where $\sin \theta \approx \theta$ is used and $m_h = 125.25$ GeV is the mass of the SM Higgs boson.

The search of a light dark scalar with $m_\phi < 5$ GeV has been conducted and proposed in various experiments (see Refs. [6, 7] for a recent review). For an electroweak-scale or higher dark phase transition, m_ϕ can readily be above $\mathcal{O}(10)$ GeV. The promising detection could then come from the Higgs invisible decay $h \rightarrow 2\phi$, if $m_\phi < m_h/2$ and $c\gamma\tau_\phi > 1$ m, with τ_ϕ the lifetime of ϕ and the decay width

$$\Gamma_{h \rightarrow 2\phi} = \frac{\lambda_p^2 v_{\text{EW}}^2 m_h^3}{32\pi(m_h^2 - m_\phi^2)^2} \left(1 + \frac{2m_\phi^2}{m_h^2}\right)^2 \sqrt{1 - \frac{4m_\phi^2}{m_h^2}}, \quad (2.7)$$

where the dependence on θ is translated into that on the portal coupling via Eq. (2.6). The current bound of the branching ratio $\text{BR}(h \rightarrow 2\phi) = \Gamma(h \rightarrow 2\phi)/\Gamma_h$ ² from CMS gives at 95% C.L. [60]:

$$\text{BR}(h \rightarrow 2\phi) < 19\%, \quad (2.8)$$

which, in the limit of $m_\phi \ll m_h$, is translated into an upper bound of the portal coupling: $\lambda_p < 0.014$. The detection from HL-LHC [61], CEPC [62] and ILC [63–65] will increase the sensitivity of the portal coupling by at least an order of magnitude.

¹In the presence of the Higgs portal coupling, the scalar ϕ from the dark gauge $U(1)_X$ sector may be detected, though we will still call ϕ by the *dark scalar* throughout.

² $\Gamma_h = \Gamma_{h,\text{SM}} + \Gamma_{h \rightarrow 2\phi}$, with $\Gamma_{h,\text{SM}} \approx 4.1$ MeV [59].

When $m_\phi > m_h/2$, the SM Higgs cannot decay into the dark scalar. In this case, the dark scalar can still be searched for via direct production, e.g., from proton-proton beams, followed by decay to SM particles. The current bounds from 13 TeV CMS [66, 67] and 13 TeV ATLAS [68–71] in the channels $pp \rightarrow \phi \rightarrow WW/ZZ/hh/\ell\ell$ have set an upper limit on the mixing angle θ at the level of 0.1, while the future upcoming/proposed experiments will further increase the sensitivity of the mixing angle. In particular, the future 14 TeV muon collider with an integrated luminosity 14 ab^{-1} can probe a mixing angle at the level of 0.01 via the decay channel $\phi \rightarrow 2h$ [72].

For $m_\phi > m_h/2$, on the other hand, indirect signals of the heavy dark scalar from collider experiments can also be probed. A simple and powerful way is to consider the signal/coupling strength modifier, defined via the cross section times the branching ratio in the narrow-width approximation [73],

$$\sigma(i \rightarrow h)\text{BR}(h \rightarrow f) \equiv \mu_i^f \times (\sigma_{i,\text{SM}}\text{BR}_{h \rightarrow f,\text{SM}}) \equiv \frac{(\sigma_{i,\text{SM}} \times \kappa_i^2)(\Gamma_{h \rightarrow f,\text{SM}} \times \kappa_f^2)}{\Gamma_{h,\text{SM}} \times \kappa_h^2}. \quad (2.9)$$

The signal strength modifier μ_i^f with initial/final state i/f characterizes the deviation from the SM prediction in a given channel $i \rightarrow h \rightarrow f$, while the coupling strength modifier κ_i is used to describe the deviations of the SM Higgs boson couplings to the SM fermions/gauge bosons, with $\kappa_h^2 \equiv \sum_j \kappa_j^2 \Gamma_{h \rightarrow j,\text{SM}}/\Gamma_{h,\text{SM}}$. In the dark $U(1)_X$ scenario, the scalar-Higgs mixing induces a universal coupling strength modifier: $\kappa_i^2 = \cos^2\theta = \kappa_h^2$, and a universal signal strength modifier: $\mu_i^f = \cos^2\theta \equiv \mu$. The current measurements of a universal μ from ATLAS and CMS set $\sin\theta \lesssim 0.3$ at 95% C.L. [74, 75], while the future electron-positron colliders, such as ILC, CEPC and FCC-ee, can reach a κ_Z precision of the ZZh coupling at the level of 0.1% [61, 76]. With the uncertainty at 2σ level, it implies that a mixing angle down to the level of 0.06 can be probed.

It is noteworthy that a universal coupling strength modifier is a characteristic feature for the dark scalar singlet, which can itself serve as a distinguishable property from variant scalar-extended scenarios, such as the two-Higgs-doublet models [77, 78].

Before going to another window associated with the direct detection of DM in Sec. 3.2, let us now turn to a fundamental setup for the dark evolution in the early universe, which is relevant for the dynamics of the dark phase transition and the DM freeze-out.

2.3 Higgs portal for dark thermalization

Besides opening the detection channels of the minimal dark sector at colliders, the Higgs portal coupling also plays an important role in dark thermalization. In the early universe, the minimal dark sector could share a common temperature with the SM thermal bath before the dark phase transition, if the portal coupling is sufficiently large. It could also be the case that the dark sector has a different temperature from the SM one due to, e.g., an asymmetric reheating dynamics from the very beginning of the early universe after inflation, or an early decoupling before the dark phase transition. However, when the dark sector is colder than the SM plasma, with a temperature ratio $\xi \equiv T_D/T_{\text{SM}} < 1$, the vacuum energy release during the first-order phase transition would be suppressed by ξ^4 [19], and in

particular, the sound-wave dominated GW peak amplitude would be suppressed by ξ^8 [22], making the GW signal harder to detect. Therefore, a large enough portal coupling is favored to ensure a hot dark plasma that can generate strong GW signals.

The lower limit of λ_p for a common temperature ($\xi = 1$, or one-temperature treatment) between the dark and the SM sectors can be derived as follows. Before the electroweak and dark gauge symmetry breaking, the dominant thermalization process comes from the quartic scalar-Higgs scattering: $2H \rightarrow 2S$. The collision rate can be written as [79]:

$$\gamma_{2H \rightarrow 2S} = \frac{T}{32\pi^4} \int_{\hat{s}_{\min}}^{\infty} d\hat{s} \sqrt{\hat{s}} (\hat{s} - 4m_H^2) K_1(\sqrt{\hat{s}}/T) \sigma_{2H \rightarrow 2S}, \quad (2.10)$$

where $\hat{s}_{\min} = \max[4m_H^2, 4m_S^2]$ with $m_H \approx 0.4T$ [80] the SM Higgs thermal mass and $m_S^2(T) \approx g_X^2 T^2/4$ the thermal mass of the dark scalar³. K_1 is the modified Bessel function, and the cross section is given by

$$\sigma_{2H \rightarrow 2S} = \frac{\lambda_p^2 \beta_S}{16\pi \beta_H \hat{s}}, \quad (2.11)$$

where $\beta_{S,H} \equiv \sqrt{1 - 4m_{S,H}^2(T)/\hat{s}}$. The thermalization condition for the one-temperature treatment of the dark phase transition requires that the thermally averaged rate $\langle \sigma v \rangle n \equiv \gamma_{2H \rightarrow 2S}/n_{\text{eq}}$, with $n_{\text{eq}} \approx 0.12T^3$ the thermal scalar number density, should be larger than the Hubble rate,

$$\mathcal{H} = \sqrt{\frac{4\pi^3}{45} g_\rho(T)} \frac{T^2}{M_{\text{Pl}}}, \quad (2.12)$$

before the phase transition completes. Here, $g_\rho(T)$ is the relativistic degrees of freedom for energy density and $M_{\text{Pl}} = 1.22 \times 10^{19}$ GeV the Planck mass. A lower bound of the portal coupling can then be derived by $\langle \sigma v \rangle n > \mathcal{H}$. Neglecting the β_S dependence, we obtain a simple lower bound of λ_p in terms of the temperature,

$$\lambda_p \gtrsim 9.5 \times 10^{-8} \left(\frac{T}{\text{GeV}} \right)^{1/2}, \quad (2.13)$$

where $g_\rho(T) = 110.75$ is used as a reference. From Eq. (2.13), we can see that for an electroweak-scale dark phase transition, $\lambda_p > \mathcal{O}(10^{-6})$ is required.

After the dark phase transition and the gauge symmetry breaking, the dark scalar can either be in thermal equilibrium or go out of equilibrium. Requiring the SM and the DM to be still in thermal equilibrium prior to the DM freeze-out is the simplest and most minimal setup to derive the DM dynamics, as will be considered here. The DM freeze-out in the one-temperature treatment requires that before the freeze-out temperature at $T_{\text{fo}} \simeq m_{A'}/25$, the dark scalar should keep A'_μ in thermal equilibrium via scalar-SM interactions. Depending on T_{fo} and m_ϕ , the dominant process keeping ϕ in thermal contact with the SM plasma can come either from two-body scalar-fermion or from two-body scalar-boson process, such as

³This can be derived by $\partial^2 V_{\text{eff}}(\varphi, T)/\partial\varphi^2$ with $V_{\text{eff}}(\varphi, T)$ given in (4.1) or (A.5).

$\phi \rightleftharpoons b\bar{b}$ or $\phi \rightleftharpoons 2h$. To follow the one-temperature freeze-out, the thermally averaged decay rate should be larger than the Hubble parameter before T_{fo} .

For $T_{\text{fo}} \sim \mathcal{O}(1-10)$ GeV and $m_h > m_\phi > m_h/2$, we evaluate the thermal condition via $\phi \rightleftharpoons b\bar{b}$, with the vacuum decay width

$$\Gamma_{\phi \rightarrow b\bar{b}} = \frac{3\theta^2 m_b^2}{8\pi v_{\text{EW}}^2} m_\phi \left(1 - \frac{4m_b^2}{m_\phi^2}\right)^{3/2}, \quad (2.14)$$

where m_b is the mass of the bottom quark. The thermally averaged decay rate reads

$$\langle \Gamma_{\phi \rightarrow b\bar{b}} \rangle \equiv \frac{1}{n_{\phi, \text{eq}}} \int d\Pi_\phi d\Pi_b d\Pi_{\bar{b}} f_\phi |\mathcal{M}|_{\phi \rightarrow b\bar{b}}^2 (2\pi)^4 \delta^4(p_\phi - p_b - p_{\bar{b}}) \quad (2.15)$$

$$\approx \Gamma_{\phi \rightarrow b\bar{b}} \frac{K_1(m_\phi/T)}{K_2(m_\phi/T)}, \quad (2.16)$$

where $d\Pi_i \equiv d^3p_i / [(2\pi)^3 2E_i]$ is the phase-space factor and $n_{\phi, \text{eq}}$ denotes the thermal number density of the dark scalar. The second line in the above equation is obtained by taking the Boltzmann approximation $f_\phi = e^{-E_\phi/T}$.⁴

For $T_{\text{fo}} \gg 10$ GeV and $m_\phi > 2m_h$, we evaluate the thermal condition via $\phi \rightleftharpoons 2h$, with the vacuum decay width

$$\Gamma_{\phi \rightarrow 2h} = \frac{\theta^2 m_\phi^3}{32\pi v_{\text{EW}}^2} \left(1 - \frac{4m_h^2}{m_\phi^2}\right)^{1/2} \left(1 + \frac{2m_h^2}{m_\phi^2}\right)^2. \quad (2.17)$$

The thermally averaged decay rate reads

$$\langle \Gamma_{\phi \rightarrow 2h} \rangle \equiv \frac{1}{n_{\phi, \text{eq}}} \int d\Pi_\phi d\Pi_h d\Pi_h f_\phi |\mathcal{M}|_{\phi \rightarrow 2h}^2 (2\pi)^4 \delta^4(p_\phi - p_h - p_h) \quad (2.18)$$

$$\approx \Gamma_{\phi \rightarrow 2h} \frac{K_1(m_\phi/T)}{K_2(m_\phi/T)}. \quad (2.19)$$

The one-temperature condition for the DM freeze-out then requires

$$\left. \frac{\langle \Gamma_{\phi \rightarrow b\bar{b}} \rangle}{\mathcal{H}} \right|_{T=T_{\text{fo}}} > 1, \quad \text{or} \quad \left. \frac{\langle \Gamma_{\phi \rightarrow 2h} \rangle}{\mathcal{H}} \right|_{T=T_{\text{fo}}} > 1. \quad (2.20)$$

Thus far, we have seen that a large enough portal coupling is favored for detection and thermalization of the dark sector. Besides, when the gauge boson is a stable DM candidate, the Higgs portal also induces interactions between the SM particles and the gauge boson, and in particular, the interaction between nucleon and DM. We will show in Sec. 3.2 that the DM direct detection via nucleon-DM scattering also sets severe bounds on the Higgs portal coupling, while the future sensitivity from, e.g., the LZ experiment will be able to test such a minimal dark sector.

⁴When the complementary tests are concerned in Sec. 6, this approximation suffices to derive the bounds of the Higgs portal coupling.

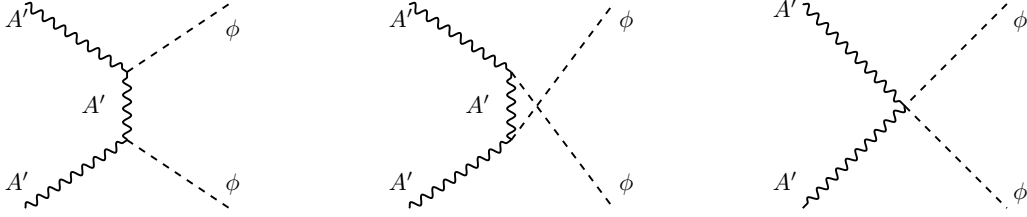


Figure 1. The dominant annihilation processes for the gauge boson DM freeze-out.

3 Dark gauge boson as WIMP-like DM

3.1 Relic density

If the dark scalar is thermalized via the Higgs portal coupling, the strong interaction in the dark sector can further keep the dark gauge boson in thermal equilibrium. Afterwards, the gauge boson DM undergoes freeze-out via annihilation to the dark scalar. The freeze-out process to determine the DM relic density is via $2A'_\mu \rightarrow 2\phi$, with the Feynman diagrams shown in Fig. 1. It is noteworthy that the vector DM A'_μ can also have a portal interaction with the SM Higgs via $h^2 A'_\mu A'^\mu$, which was considered in Refs. [54, 81, 82] as the dominant portal for a vector DM and could be induced by integrating out a heavy dark scalar at tree level via the Higgs portal. Since we are interested in a small Higgs portal coupling, the dominant processes to determine the DM freeze-out reduce to the dark interaction shown in Fig. 1.

The Boltzmann equation for the dark gauge boson freeze-out is given by

$$\frac{dY_{A'}}{dx} = -\frac{s\langle\sigma v\rangle_{A'}}{\mathcal{H}x} \left(Y_{A'}^2 - \frac{Y_\phi^2}{Y_{\phi,\text{eq}}^2} Y_{A',\text{eq}}^2 \right), \quad (3.1)$$

where the yield is defined as $Y_{A',\phi} \equiv n_{A',\phi}/s$ and $x \equiv m_{A'}/T$. The entropy density is given by

$$s = \frac{2\pi^2}{45} g_s(T) T^3, \quad (3.2)$$

with $g_s(T)$ the relativistic degrees of freedom for entropy density in the plasma, and the Hubble parameter \mathcal{H} is given by Eq. (2.12). The thermally averaged cross section of DM annihilation can be defined as

$$\langle\sigma v\rangle_{A'} \equiv 2(a + 3b/x), \quad (3.3)$$

where we add a factor of 2 to take into account the pair DM annihilation, with the expressions of a and b collected in Appendix B.

Under the one-temperature regime, the scalar is still in thermal equilibrium when the gauge boson starts to freeze out. Therefore we take $Y_\phi \approx Y_{\phi,\text{eq}}$ in Eq. (3.1). Following the standard semi-analytic approach [83], we can parameterize the departure from equilibrium by $\Delta \equiv Y_{A'} - Y_{A',\text{eq}}$. The Boltzmann equation for Δ is then given by

$$\frac{d\Delta}{dx} = -\frac{dY_{A',\text{eq}}}{dx} - \frac{s\langle\sigma v\rangle_{A'}}{\mathcal{H}x} \Delta[\Delta + 2Y_{A',\text{eq}}]. \quad (3.4)$$

Before the gauge boson departs from chemical equilibrium, the change of Δ is small, so that we can write

$$\Delta = -\frac{dY_{A',\text{eq}}}{dx} \frac{\mathcal{H}x}{s\langle\sigma v\rangle_{A'}} \frac{1}{\Delta + 2Y_{A',\text{eq}}}. \quad (3.5)$$

During the freeze-out, $Y_{A'}$ departs significantly from $Y_{A',\text{eq}}$ so that Δ is comparable to $Y_{A',\text{eq}}$. Defining $\Delta \equiv cY_{A',\text{eq}}$ at freeze-out, with an order-one constant c determined by numerical matching, we can derive the freeze-out temperature from Eq. (3.5) as

$$x_f = \ln \left(\sqrt{\frac{45}{2}} \frac{c(c+2)}{4\pi^3} \frac{g_s g_{A'}}{g_\rho^{3/2}} M_{\text{Pl}} m_{A'} \frac{\langle\sigma v\rangle_{A'}}{\sqrt{x_f} [1 - 3/(2x_f)]} \right), \quad (3.6)$$

where $g_{A'} = 3$ is the internal degrees of freedom for the massive gauge boson and we have used the thermal yield of the nonrelativistic A'_μ ,

$$Y_{A',\text{eq}} = \frac{45 g_{A'} x^{3/2} e^{-x}}{4\sqrt{2}\pi^{7/2} g_s(T)}. \quad (3.7)$$

Towards the end of freeze-out, Δ turns to be constant while $Y_{A',\text{eq}}$ becomes negligible due to Boltzmann suppression. During this stage, we can obtain a simple equation of Δ from Eq. (3.4) as

$$d\Delta^{-1} = \frac{s\langle\sigma v\rangle_{A'}}{\mathcal{H}x} dx. \quad (3.8)$$

The final abundance of A'_μ is given by integrating x in the above equation from $x = x_f$ to $x = \infty$, leading to

$$Y_{A'}(x = \infty) \approx \Delta(x = \infty) = \left(\int_{x_f}^{\infty} \frac{s\langle\sigma v\rangle_{A'}}{\mathcal{H}x} dx + [cY_{A',\text{eq}}]^{-1} \Big|_{x_f} \right)^{-1}. \quad (3.9)$$

The relic density is given by

$$\Omega_{\text{DM}} h^2 = \frac{s_0 m_{A'}}{\rho_c / h^2} Y_{A'}(x = \infty), \quad (3.10)$$

with the current entropy density $s_0 = 2891.2 \text{ cm}^{-3}$ and the critical density today $\rho_c = 1.05 \times 10^{-5} \cdot h^2 \cdot \text{GeV} \cdot \text{cm}^{-3}$ [84].

Since a strong first-order phase transition favors $m_{A'} > m_\phi$, the DM relic density depends essentially on $m_{A'}$ and g_X only. Matching the observed value $\Omega h^2 \approx 0.12$ [85] then allows us to remove one of these free parameters. To this end, we approximate the freeze-out temperature as

$$x_f \approx 42.83 + \ln \left(\frac{g_X^4}{\sqrt{g_{\text{eff}}}} \frac{\text{GeV}}{m_{A'}} \right), \quad (3.11)$$

where we have taken $c \approx 0.4$ [83], $x_f \approx 25$ and $g_{\text{eff}} \equiv g_s \approx g_\rho$ in the logarithmic function of Eq. (3.6), though x_f can be numerically solved by iteration. It can be seen that for

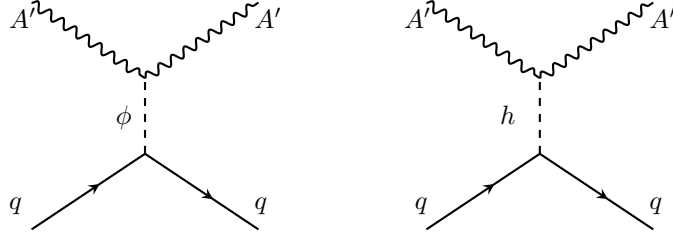


Figure 2. The DM-nucleon scattering mediated by the dark scalar ϕ and the SM Higgs boson h , where q denotes the quark component in the nucleon.

an electroweak A'_μ and a weak coupling g_X , the freeze-out temperature is expected to be around $x_f \approx 25$.

The relic density can be approximated as

$$\left(\frac{\Omega_{\text{DM}} h^2}{0.12}\right) \approx 0.33 \left(\frac{0.1}{g_X}\right)^4 \left(\frac{m_{A'}}{100 \text{ GeV}}\right)^2, \quad (3.12)$$

where we have taken a benchmark value $g_{\text{eff}} = 80$, corresponding to a freeze-out temperature around $\mathcal{O}(10 - 100)$ GeV and hence $m_{A'} \simeq \mathcal{O}(100 - 1000)$ GeV. We will use Eq. (3.12), or equivalently

$$m_{A'} \approx 1.75 \times 10^4 g_X^2 \text{ GeV}, \quad v_\phi \approx 1.75 \times 10^4 g_X \text{ GeV}, \quad (3.13)$$

as a numerical approximation to remove the dependence of the dark phase transition on $m_{A'}$ and v_ϕ .

As will be shown in this paper, $0.1 < g_X < 1$ and $10^{-4} < \lambda \ll 1$ are favored for a strong first-order dark phase transition and observable GW signals. Under this circumstance, the DM mass is predicted to be around 100 GeV–10 TeV, which is below the perturbative unitarity bound at $\mathcal{O}(100)$ TeV [86], while the high-energy elastic scattering matrices for the longitudinal gauge boson (or equivalently χ) and the dark scalar ϕ can also readily satisfy the unitarity constraint due to a small quartic coupling λ [87].

3.2 Higgs portal for DM direct detection

The dark gauge boson DM can interact with the SM fermions via the scalar-Higgs mixing induced coupling. The direct detection via scattering between DM and nucleons has been conducted in LUX [39], XENON1T [40], PandaX-II [41], PandaX-4T [42] and LZ [43] experiments. The null observations from these experiments have set severe bounds in the spin-independent cross section in terms of the DM mass. Future sensitivity from LZ [49, 50] and DARWIN [88, 89] will further improve the cross section limit by at least two orders of magnitude.

The scattering between the DM A'_μ and the nucleons goes through the t channel mediated by the two physical scalar states, i.e., ϕ and h , as shown in Fig. 2. The spin-independent cross section is straightforward to obtain, giving

$$\sigma_{A'N} = \frac{f^2 g_X^4 v_\phi^2 \theta^2}{\pi v_{\text{EW}}^2} \frac{m_N^4 (m_h^2 - m_\phi^2)^2}{m_h^4 m_\phi^4 (m_N + m_{A'})^2} = \frac{f^2 \lambda_p^2 m_{A'}^4 m_N^4}{\pi m_h^4 m_\phi^4 (m_N + m_{A'})^2}, \quad (3.14)$$

where m_N is the nucleon mass⁵ and we use $f \approx 0.3$ [91, 92] as the effective Higgs-proton (neutron) coupling from the nucleon matrix elements $f \equiv \sum_q \langle N | m_q q \bar{q} / m_N | N \rangle$. Note that, we have neglected the recoil energy dependence in the dark scalar propagator. This approximation will be justified in Sec. 6 where a strong first-order phase transition typically predicts $m_\phi > \mu_{A'N} E_R$, with $\mu_{A'N} \equiv m_{A'} m_N / (m_{A'} + m_N)$ the reduced DM-nucleon mass and E_R the recoil energy.

For the one-temperature freeze-out, the dark gauge boson acts as a DM particle between the standard WIMP and the secluded WIMP paradigms [2], since the annihilation product is within the dark sector rather than the SM particles and the coupling fixing the relic density is largely disentangled from that controlling the DM-nucleon cross section. Under this circumstance, the tension between the null observations and the standard WIMP prediction can readily be alleviated via a small mixing angle θ . However, since a sufficiently large portal coupling is favored for detection and strong GW signals, it is interesting to investigate the favored ranges of λ_p which can explain the current null observations and at the same time predict a DM-nucleon cross section detectable by future experiments above the notorious neutrino floor [52, 53]. This is one of the main purposes in this paper, as we shall discuss in Sec. 6.

3.3 Higgs portal for DM indirect detection

As mentioned above, the dominant DM annihilation channel is the dark scalar product, while the cross sections of annihilation to SM particles are expected to be suppressed by the portal coupling λ_p and the mass ratio $m_{\text{SM}}/m_{A'}$. In this case, a significant indirect signal of DM annihilation at present day could still be feasible if the annihilation cross sections are boosted by the Sommerfeld enhancement [93] for low DM velocities ($v \simeq \mathcal{O}(10-1000)\text{km/s}$) in the regions of typical dwarf galaxies or galaxy clusters [94].

The Sommerfeld effect is a non-relativistic quantum effect, arising from a force carrier between the incoming particles. The force carrier, or the mediator between the two non-relativistic particles, can distort the incoming wave functions away from the plane-wave approximation, potentially yielding enhancement or suppression to annihilation cross section. In the minimal $U(1)_X$ scenario, the dark scalar ϕ plays the role of mediator between two gauge bosons A'_μ . For the Sommerfeld effect to be significant, however, the mass hierarchy between ϕ and A'_μ should typically satisfy the following condition [95–98]:

$$m_\phi \lesssim \alpha_X m_{A'} , \quad (3.15)$$

where $\alpha_X \equiv g_X^2/(4\pi)$. The above condition reduces to

$$\lambda \lesssim \frac{g_X^6}{32\pi^2} . \quad (3.16)$$

⁵Usually the measured DM-nuclear cross section has been reduced by defining an effective per-nucleon cross section so as to facilitate comparison between different experiments with different nuclei (such as xenon in the LZ experiment) [90]. Therefore, we will take the nucleon mass $m_N \approx 0.931$ GeV to evaluate the effective DM-nucleon cross section in Eq. (3.14) without the quadratic scaling of the atomic mass number, and compare with the excluded cross section.

So one can expect that the Sommerfeld effect only arises when the self-interacting coupling of the dark scalar is much smaller than the gauge coupling.

To estimate the DM annihilation cross section to SM particles, let us consider the dominant channel $2A'_\mu \rightarrow t\bar{t}$. The process is mediated by the Higgs boson and the dark scalar in the s channel, the cross section of which reads

$$(\sigma v)_{A' \rightarrow t} \approx \frac{\lambda_p^2 m_t^2}{512\pi m_{A'}^4} \propto \left(\frac{\lambda_p}{g_X^2}\right)^2 \left(\frac{m_t}{m_{A'}}\right)^2 (\sigma v)_{A' \rightarrow \phi}. \quad (3.17)$$

The above result corresponds to the s -wave approximation in the limit $m_{A'} > m_\phi, m_t$, with m_t the top-quark mass. Besides, we have used Eq. (2.6) and Eq. (B.4) for $(\sigma v)_{A' \rightarrow \phi}$. We can see that, comparing the $2A'_\mu \rightarrow 2\phi$, $(\sigma v)_{A' \rightarrow t}$ would be much suppressed for $m_{A'} \gg m_t$ and $g_X^2 \gg \lambda_p$.

Therefore, without a significant Sommerfeld enhancement, the indirect signals of DM via annihilation to SM particles or via annihilation to dark scalar followed by decay to SM particles can hardly be detected. We will find out in Sec. 6 that Eq. (3.15) or Eq. (3.16) is in general not satisfied when observational GW signals are concerned.

4 Dark phase transition from a minimal hot boson plasma

The dark scalar potential (2.1) at finite temperatures in the early universe could exhibit a global minimum at $\langle S \rangle = 0$ rather than $\langle S \rangle = v_\phi$ such that the gauge $U(1)_X$ symmetry is maintained above some critical temperature T_c . At T_c , which is defined by the epoch when there are degenerate vacua such that $V(\langle S \rangle_1) = V(\langle S \rangle_2)$, another minimum of the potential at $\langle S \rangle \neq 0$ arises. The two degenerate vacua are separated by an energy barrier, which is a necessary condition for a strong first-order phase transition. At some temperatures just below T_c , the quantum/thermal tunneling from the false to true vacuum occurs, and a first-order phase transition begins, followed by spontaneous gauge symmetry breaking. A common practice for the dynamics of the phase transition is the effective potential analysis, as we shall describe in this section.

4.1 Effective potential

The effective potential in the dark boson plasma can be generically written as

$$V_{\text{eff}}(\varphi, T) = V_0 + V_{\text{CW}} + V_{\text{CT}} + V_T + V_{\text{daisy}}, \quad (4.1)$$

where the tree-level potential for the background field φ at zero temperature is given by

$$V_0(\varphi) = -\frac{1}{2}\mu_S^2\varphi^2 + \frac{\lambda}{4}\varphi^4, \quad (4.2)$$

and the tree-level φ -dependent masses of the quantum fields read

$$m_\phi^2(\varphi) = -\mu_S^2 + 3\lambda\varphi^2, \quad m_\chi^2(\varphi) = -\mu_S^2 + \lambda\varphi^2, \quad m_{A'}^2(\varphi) = g_X^2\varphi^2. \quad (4.3)$$

The zero-temperature Coleman-Weinberg potential $V_{\text{CW}}(\varphi)$ is induced by the quantum scalar fields ϕ, χ and the gauge vector field A'_μ . In the Landau gauge with the $\overline{\text{MS}}$ renormalization scheme, $V_{\text{CW}}(\varphi)$ reads [34]

$$V_{\text{CW}}(\varphi) = \frac{1}{64\pi^2} \sum_{i=\phi,\chi,A'} n_i m_i^4(\varphi) \left[\ln \left(\frac{m_i^2(\varphi)}{\mu^2} \right) - C_i \right], \quad (4.4)$$

where μ is the renormalization scale⁶, $n_\phi = n_\chi = 1, n_{A'} = 3$ accounts for the internal degrees of freedom, and $C_{\phi,\chi} = 3/2, C_X = 5/6$ are the renormalization-dependent constants.

There are notorious IR issues associated with the massless Goldstone boson χ in the Coleman-Weinberg loop function. It can be clearly seen that when the tree-level mass of m_χ from Eq. (4.3) in vacuum $\varphi = v_\phi$ is taken, there would be a divergence in the logarithmic function. It can also be seen that when the vacuum mass of ϕ is determined by adding loop corrections, i.e., $\partial^2(V_0 + V_{\text{CW}})/\partial\varphi^2|_{\varphi=v_\phi} = m_\phi^2$, we will encounter the logarithmic divergence due to the second derivative of V_{CW} at $\varphi = v_\phi$. While there are several ways to evade a massless Goldstone boson [99–101], we will simply drop the contribution from χ [102] in the following analysis. This approximation is reasonable for a minimal dark boson plasma, where the dominant contribution to induce a strong first-order phase transition comes from the gauge boson, with $\lambda \ll g_X^2$.

The counterterm $V_{\text{CT}} \equiv -\delta\mu_S^2\varphi^2/2 + \delta\lambda^4\varphi^4/4$ is chosen to maintain the tree-level vacuum and mass conditions of ϕ , such that

$$\left. \frac{\partial(V_{\text{CW}} + V_{\text{CT}})}{\partial\varphi} \right|_{\varphi=v_\phi} = 0, \quad \left. \frac{\partial^2(V_{\text{CW}} + V_{\text{CT}})}{\partial\varphi^2} \right|_{\varphi=v_\phi} = 0, \quad (4.5)$$

leading to

$$\begin{aligned} V_{\text{CT}} = & \frac{3v_\phi^2}{64\pi^2} \left[2g_X^4 + 2\lambda^2 \ln \left(\frac{m_\phi^2}{\mu^2} \right) + 7\lambda^2 \right] \varphi^2 \\ & - \frac{3}{128\pi^2} \left[3g_X^4 + 2g_X^4 \ln \left(\frac{m_{A'}^2}{\mu^2} \right) + 9\lambda^2 + 6\lambda^2 \ln \left(\frac{m_\phi^2}{\mu^2} \right) \right] \varphi^4, \end{aligned} \quad (4.6)$$

where the masses in the logarithmic function are given by Eqs. (2.3) and (2.5).

The finite-temperature potential from ϕ, χ and A'_μ is given by

$$V_T = \frac{T^4}{2\pi^2} \sum_{i=\phi,\chi,A'} n_i J_B(x_i), \quad (4.7)$$

where J_B reads

$$J_B(x_i) = \int_0^\infty y^2 dy \ln \left(1 - e^{-\sqrt{y^2 + x_i^2}} \right), \quad (4.8)$$

⁶We fix the scale by $\mu = v_\phi$ throughout. Since λ and g_X are treated as free parameters in this paper, we will not consider the renormalization dependence of $V_{\text{eff}}(\varphi, T)$ in numerical analyses.

with $x_i \equiv m_i(\varphi)/T$. Note that there is no fermion integral J_F in V_T as we consider a minimal dark boson plasma. For the numerical analysis, we keep V_T without expanding in the high-temperature limit. An analytic analysis with the high-temperature expansion will be presented in Appendix A.

Besides the finite-temperature corrections presented in Eq. (4.7), there are significant corrections from daisy rings. Following the Arnold-Espinosa resummation [103], we can write the daisy potential from the gauge boson as

$$V_{\text{daisy}} = -\frac{g_X^3 T}{12\pi} \left[\left(\varphi^2 + \frac{T^2}{3} \right)^{3/2} - \varphi^3 \right], \quad (4.9)$$

which corresponds to the mass replacement:

$$m_{A',T(L)}^2(\varphi, T=0) \rightarrow m_{A',T(L)}^2(\varphi, T=0) + c_{T(L)} g_X^2 T^2, \quad (4.10)$$

with $c_T = 0, c_L = 1/3$ for the transverse and longitudinal components of A'_μ [10, 58]. The thermal mass corrections to scalars can also be included similarly. Nevertheless, we will neglect the scalar contributions to the dark phase transition, which is a good approximation as long as the gauge coupling g_X is much larger than the scalar coupling λ .

4.2 Dynamics of dark phase transition

During the phase transition, the true-vacuum bubbles start to nucleate when the thermal tunneling probability per Hubble time and per Hubble volume is at order unity. The nucleation temperature T_n can be defined by [104, 105]:

$$\Gamma(T_n) \simeq T_n^4 e^{-S_3/T_n} \simeq \mathcal{H}^4(T_n), \quad (4.11)$$

where the Hubble parameter is given by Eq. (2.12). S_3 is the three-dimensional Euclidean action,

$$S_3 = 4\pi \int_0^\infty r^2 dr \left[\frac{1}{2} \left(\frac{d\varphi}{dr} \right)^2 + V_{\text{eff}}(\varphi, T) \right], \quad (4.12)$$

where the effective potential is given by Eq. (4.1) and the background field $\varphi(r)$ is the $O(3)$ -symmetric bounce solution to the equation of motion:

$$\frac{d^2\varphi}{dr^2} + \frac{2}{r} \frac{d\varphi}{dr} = \frac{dV_{\text{eff}}}{d\varphi}, \quad (4.13)$$

satisfying the boundary conditions

$$\lim_{r \rightarrow \infty} \varphi(r) = 0, \quad \left. \frac{d\varphi(r)}{dr} \right|_{r=0} = 0. \quad (4.14)$$

The nucleation temperature from Eq. (4.11) can be rewritten as

$$\frac{S_3(T_n)}{T_n} = 146 - 2 \ln \left(\frac{g_\rho(T_n)}{100} \right) - 4 \ln \left(\frac{T_n}{100 \text{ GeV}} \right). \quad (4.15)$$

To compute the nucleation temperature, one should solve the bounce equation (4.13), which in general can be done by numerical approaches. To this end, we use the Python package `CosmoTransitions` [106] to calculate the Euclidean action S_3 and then determine the nucleation temperature via Eq. (4.15)⁷.

When associated with the GW profiles, the strength of the phase transition is usually characterized by the α parameter, which is defined by the difference of the trace anomaly from the total energy-momentum tensor over the energy density in the symmetric phase [44, 107]:

$$\alpha = \frac{1}{\rho_R} \left(\Delta V_{\text{eff}} - \frac{T}{4} \frac{\partial \Delta V_{\text{eff}}}{\partial T} \right), \quad (4.16)$$

where the radiation energy density ρ_R in the plasma is given by

$$\rho_R = \frac{\pi^2 g_\rho(T)}{30} T^4, \quad (4.17)$$

and ΔV_{eff} is the potential difference between the false and true vacua: $V_{\text{eff}}(\varphi_{\text{false}}, T) - V_{\text{eff}}(\varphi_{\text{true}}, T) > 0$.

Another important parameter describing the GW profiles is the so-called β -parameter, which is defined by the time derivative of the exponent in the thermal tunneling probability per unit time and per unit volume, i.e.,

$$\beta = -\frac{d}{dt} \left(\frac{S_3}{T} \right) = \mathcal{H} T \frac{d}{dT} \left(\frac{S_3}{T} \right), \quad (4.18)$$

where the relation $dT/dt = -\mathcal{H}T$ at the radiation-dominated epoch is used in the second equation. Then the ratio β/\mathcal{H} at T_n can be expressed as

$$\frac{\beta}{\mathcal{H}} = T \frac{d}{dT} \left(\frac{S_3}{T} \right) \Big|_{T_n}. \quad (4.19)$$

Note that the GW production is usually evaluated at the percolation temperature T_p , which is approximately equal to the temperature at the time of the bubble nucleation, $T_p \approx T_n$, unless the phase transition occurs in a strongly supercooled state with $\alpha \gg 1$ [15, 16]. In this work, we will confine ourselves to $\alpha < 1$ and use the approximation $T_* \approx T_n$ to describe the GW profiles.

5 GW profiles

In general, there are three types of phase transitions: (i) non-runaway phase transition in a plasma, (ii) runaway phase transition in a plasma, and (iii) runaway phase transition in vacuum. The last situation generically predicts $\alpha \gg 1$ and hence exhibits a supercooled regime. When the supercooling occurs, one is further required to check if the phase transition can successfully complete, which is not automatically satisfied in a given model. For

⁷Numerically, we fix $g_\rho(T_n) = 110.75$ and $T_n = 100$ GeV in the logarithmic functions of Eq. (4.15) to get a fast evaluation of T_n in `CosmoTransitions`. The resulting T_n different from $T_n = 100$ GeV by a factor of few is bearable due to the moderate logarithmic dependence.

the concern in this work, we will consider $\alpha < 1$. To further specify if the dark phase transition is a runaway or non-runaway type, one may compare α with the threshold value α_∞ [108]⁸:

$$\alpha_\infty \approx \frac{90g^2}{24\pi^2 g_\rho(T_n)} \left(\frac{\varphi_{\text{true}}(T_n)}{T_n} \right)^2, \quad (5.1)$$

at which the wall of the scalar-field bubble begins to run away at the speed of light $v_w = 1$. Usually it is thought that runaway phase transition occurs for $\alpha > \alpha_\infty$. Nevertheless, it is recently found that the efficiency of the vacuum energy conversion into the scalar field is suppressed by additional Lorentz factor ratios [16, 109],⁹ so that the efficiency is smaller than earlier estimates. It leads to the situation where most phase transitions originally found as a runaway type now become a non-runaway type unless the phase transitions are strongly supercooled, as confirmed in Refs. [112, 113].

In this paper, we will therefore consider the non-runaway phase transition with $\alpha < 1$. For a non-runaway phase transition, the dominant source to generate the stochastic GW comes from the sound wave [114]¹⁰. The induced GW peak amplitude and peak frequency are semi-analytically fitted as [114]

$$\Omega_{\text{sw}}^{\text{peak}} h^2 \approx 2.65 \times 10^{-6} (\mathcal{H}\tau_{\text{sw}}) \left(\frac{v_w}{\beta/\mathcal{H}} \right) \left(\frac{100}{g_\rho(T_n)} \right)^{1/3} \left(\frac{\kappa_{\text{sw}}\alpha}{1+\alpha} \right)^2, \quad (5.2)$$

$$f_{\text{sw}}^{\text{peak}} \approx 1.9 \times 10^{-5} \text{ Hz} \left(\frac{g_\rho(T_n)}{100} \right)^{1/6} \left(\frac{T_n}{100 \text{ GeV}} \right) \left(\frac{\beta/\mathcal{H}}{v_w} \right), \quad (5.3)$$

where we have taken into account the suppression factor $\mathcal{H}\tau_{\text{sw}} = \min(1, \mathcal{H}R_*/\bar{U}_f)$ [116–118] due to the finite lifetime of the sound wave,¹¹ with the mean bubble separation $R_* = v_w(8\pi)^{1/3}/\beta$ [119] and $\bar{U}_f^2 \approx 3\kappa_{\text{sw}}\alpha/[4(1+\alpha)]$ [120]. The efficiency factor κ_{sw} represents the fraction of the released vacuum energy converted into the bulk motion of the fluid. For a non-runaway phase transition, we apply the efficiency factor [108]

$$\kappa_{\text{sw}} \approx \frac{\alpha}{0.73 + 0.083\sqrt{\alpha} + \alpha}, \quad (5.4)$$

together with a wall velocity $v_w = 0.9$. After redshifting from the production at T_n , the GW spectrum $\Omega_{\text{GW}} h^2 \approx \Omega_{\text{sw}} h^2$ today is given by

$$\Omega_{\text{sw}} h^2(f) = \Omega_{\text{sw}}^{\text{peak}} h^2 \mathcal{S}_{\text{sw}}(f), \quad (5.5)$$

⁸In Eq. (5.1), we have taken only the dominant contribution from the gauge boson.

⁹See, however, Refs. [110, 111] for different perspectives.

¹⁰We will not include the magneto-hydrodynamic turbulence in this work, but the conclusion drawn in this section is generic for an efficiency factor $\epsilon < 1$ that determines how much portion of the energy from the sound wave is turbulent [115].

¹¹The suppression factor is also given as $\Upsilon(\tau_{\text{sw}}) = 1 - (1 + 2\mathcal{H}\tau_{\text{sw}})^{-1/2}$. For $\mathcal{H}\tau_{\text{sw}} < 1$ found in our numerical analysis, we arrive at $\Upsilon(\tau_{\text{sw}}) \approx \mathcal{H}\tau_{\text{sw}}$.

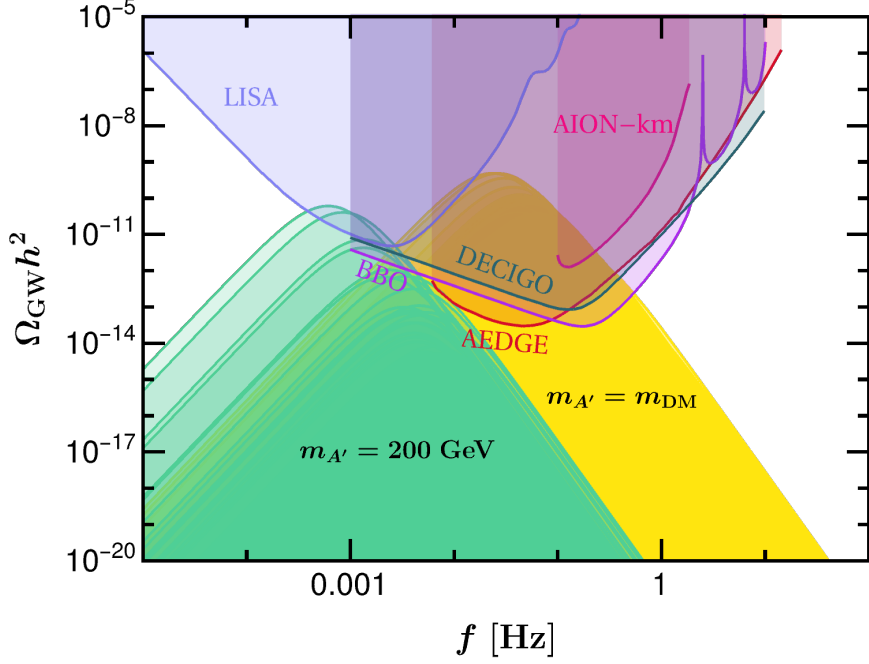


Figure 3. The GW signals induced from the dark phase transition in the minimal boson plasma under the one-temperature treatment. Also shown are the sensitivity curves from space-based interferometers, LISA [44], BBO [45], and DECIGO [46], as well as from atomic interferometers, AEDGE [48] and AION [47] from km-scale terrestrial detectors.

where $\Omega_{\text{sw}}^{\text{peak}} h^2$ is given by Eq. (5.2) and the spectral shape function \mathcal{S}_{sw} in terms of the frequency f reads

$$\mathcal{S}_{\text{sw}} = \left(\frac{f}{f_{\text{sw}}^{\text{peak}}} \right)^3 \left[\frac{7}{4 + 3(f/f_{\text{sw}}^{\text{peak}})^2} \right]^{7/2}, \quad (5.6)$$

with $f_{\text{sw}}^{\text{peak}}$ given by Eq. (5.3).

To obtain the GW curves, we perform a numerical scan of the free parameters λ, g_X in the following range¹²:

$$\lambda = 5 \times [10^{-4}, 10^{-2}], \quad g_X = [0.1, 1]. \quad (5.7)$$

The resulting $\Omega_{\text{sw}} h^2$ is shown in Fig. 3. The shaded yellow region denotes the predicted GW signals under the scan (5.7), where the DM relic density is matched to the observed value via Eq. (3.13). The peak frequencies for strong GW signals above 10^{-14} are located at 0.01 – 1 Hz. In particular, the GW curves have some overlap with the updated LISA sensitivity [44] only for large $g_X \sim 1$. This result can also be inferred from the analytic phase transition presented in Appendix A. As indicated by Eq. (5.2), a large GW amplitude favors a small β/\mathcal{H} and a large α . From the left panel of Fig. 5, we see that a small β/\mathcal{H}

¹²Using the analytic results shown in Appendix A, we find that the parameter space with $\lambda \gtrsim 0.03$ and $\lambda \lesssim 10^{-4}$ cannot generate strong enough GW signals, which is confirmed in the numerical analysis.

BP	λ	g_X	T_n	α	β/\mathcal{H}
LISA	1.7×10^{-2}	0.97	2.4 TeV	0.74	45
AION	3.0×10^{-3}	0.61	0.93 TeV	0.80	417
DECIGO	8.7×10^{-4}	0.44	0.48 TeV	0.89	1304
BBO	8.3×10^{-4}	0.43	0.58 TeV	0.30	1561

Table 1. Selected BP for GW signals detectable by LISA, AION, DECIGO and BBO, respectively.

and a large α requires a large g_X . It implies that, when A'_μ is the DM with relic density fixed via Eq. (3.13), the dark vacuum v_ϕ is at 1 – 10 TeV. In general, for a non-supercooled phase transition, we expect a nucleation temperature with the magnitude not far from the dark vacuum v_ϕ . Therefore, a large $\Omega_{\text{sw}} h^2$ favors $T_n > 100$ GeV. Then, from Eq. (5.3), we see that the peak frequency can be at $\mathcal{O}(1)$ mHz if $\beta/\mathcal{H} \lesssim 10^{13}$. However, as inferred from the left panel of Fig. 5, $\beta/\mathcal{H} < 10$ is hard to obtain, unless $g_X \gtrsim 1$. We then conclude that the inferred peak frequency for $g_X < 1$ is above $\mathcal{O}(1)$ mHz where the updated LISA sensitivity curve allows a GW amplitude as low as $\mathcal{O}(10^{-12})$. Therefore, only for some large g_X will the induced GW curves have some overlap with the detectable region from LISA.

It becomes clear that when $m_{A'}$ and g_X are disentangled by making the dark gauge boson unstable, the induced GW peak frequency can shift towards 1 mHz. Indeed, taking $m_{A'} = 200$ GeV as an example, we can see from the green region that a relatively light dark gauge boson allows more overlap with the detectable region from LISA.

When A'_μ is the DM candidate within the minimal dark boson plasma, the strong first-order phase transition can readily induce GW signals that can be detected by the space-based interferometers DECIGO [46] and BBO [45]. Furthermore, some proposed atomic interferometers can also capture the induced GW signals. This is particularly the case for the AION experiment with km-scale terrestrial detectors [47]. The space experiment AEDGE [48] that uses cold atoms to search for ultra-light DM and GW is also able to capture the GW induced from the minimal dark bosonic phase transition.

Finally, we would like to comment on the LISA sensitivity curve adopted in this paper. In fact, there are some analyses of difference LISA sensitivity curves used in the literature. In particular, the analysis based on the peak-integrated-sensitivity curves in Ref. [113] pointed out a lower curve of the LISA sensitivity. In this case, the induced GW signals from the minimal dark boson plasma would have more overlap with the estimated sensitivity region. In this paper, we do not show the peak-integrated-sensitivity curve of LISA, so our conclusions are based on the updated LISA sensitivity from Ref. [44].

¹³For $\beta/\mathcal{H} \lesssim 10$ and $0.1 < \alpha < 1$, the dark phase transition might lead to the formation of primordial black holes [121, 122]. We leave this interesting possibility for future studies.

6 Hear and see the dark: complementary tests of DM, GW and colliders

Given the current constraints and the future sensitivities, it is tempting to ask whether the parameter space for a dark first-order phase transition, observable GW signals and DM favors a Higgs portal coupling that can be probed by collider detection. To this end, we select four BP from Fig. 3, which respectively corresponds to a GW curve overlapping with the LISA region (BP for LISA), residing between LISA and AION (BP for AION), between AION and DECIGO (BP for DECIGO), and between DECIGO and BBO (BP for BBO). The parameters for each BP are shown in Tab. 1.

The first thing to notice from these BP is that, the predicted scalar masses are all above $2m_h$, so the constraints and future detection from the Higgs invisible decay are not applicable. In fact, a heavy dark scalar is generically expected when A'_μ is the DM candidate. As discussed in Sec. 5, $g_X > 0.1$ and $\lambda > 10^{-4}$ are required to induce strong GW signals. Then we can infer from Eq. (3.13) and Eq. (2.5) that the dark scalar mass is well above 10 GeV¹⁴. When A'_μ is no longer a stable DM, the dark scalar can be lighter such that the constraints and future detection of the Higgs invisible decay come into play, as discussed in Ref. [22].

For heavy dark scalar above $2m_h$, the channel $SM \rightarrow \phi \rightarrow SM$ will serve as the direct collider probe. Currently, the constraints in this channel are set by the LHC with an upper limit of θ at the level of 0.1. Future sensitivities from 3 TeV CLIC with an integrated luminosity 3 ab^{-1} in the decay channel $\phi \rightarrow 2h$ can reach a level of $\sin^2 \theta \approx 0.001$ [36, 72] and the 14 TeV muon collider with an integrated luminosity 14 ab^{-1} can further probe the mixing angle down to $\sin^2 \theta \approx 10^{-4}$ for $m_\phi < 3 \text{ TeV}$ [72]. The dashed lines shown in Fig. 4 (from right to left) correspond to the limit of θ excluded by current LHC, detectable by future CLIC and muon collider, respectively. Note that, the indirect collider probes via the coupling strength modifier κ_Z will reach a sensitivity of $\theta \simeq 0.06$, e.g., at the ILC, CEPC and FCC-ee, which is comparable with the limit reachable by direct detection from the future 3 TeV CLIC.

We show in Fig. 4 the red curve of the predicted spin-independent DM-nucleon cross section in terms of the portal coupling in each BP. The rightmost shaded region in each panel is excluded by the LZ experiment [43]¹⁵. The middle shaded region corresponds to the future LZ sensitivity [51]. The leftmost shaded region corresponds to the neutrino floor for xenon experiment [53], when the direct detection of DM suffers from irreducible background of coherent neutrino-nucleus scattering. We can see that the Higgs portal coupling down to the level of 10^{-3} can be probed by the future LZ experiment, and the spin-independent DM-nucleon cross section can reach as large as $\sigma_{A'N} \simeq \mathcal{O}(10^{-45}) \text{ cm}^2$.

Combining the GW signals, DM direct detection and the collider tests, we can see that for all the BP, the CLIC is able to test a portion of the parameter space that induces GW signals observable by LISA, AION, DECIGO and BBO, respectively. For all the panels

¹⁴It justifies the approximation of neglecting the dependence on the recoil energy in the calculation of the DM-nucleon cross section.

¹⁵Currently, the LZ experiment sets the most severe bound on the spin-independent DM-nucleon cross section. See also the very recently released constraint from the XENONnT experiment [123].

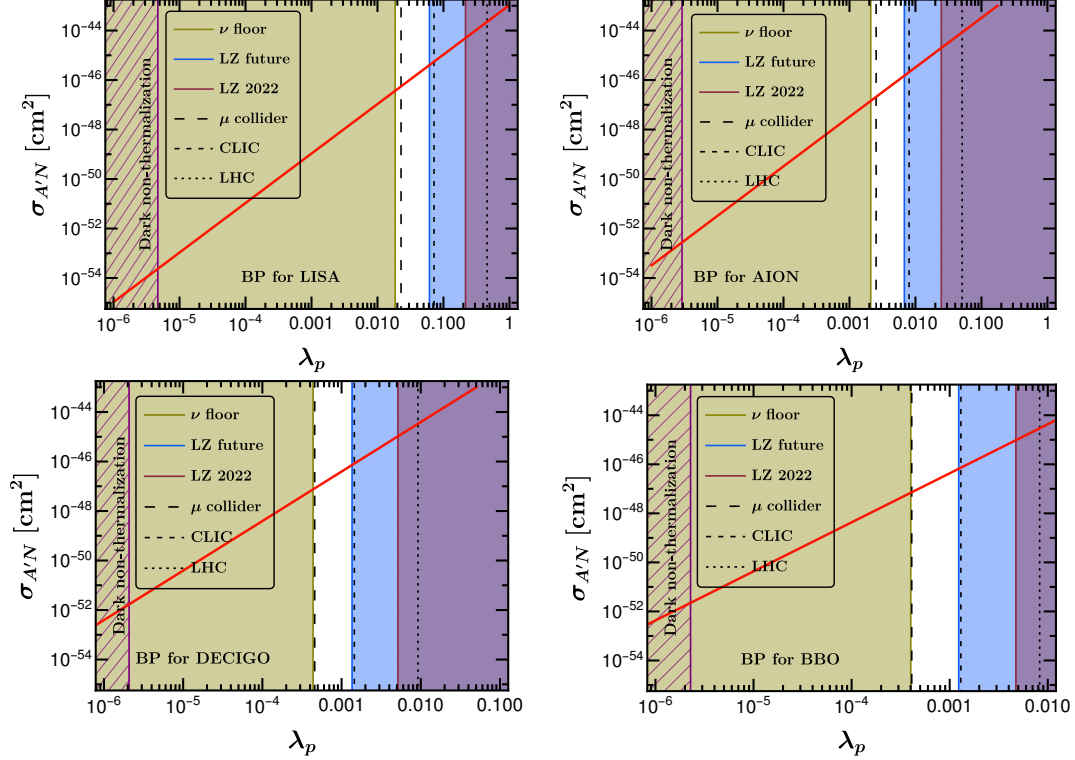


Figure 4. The parameter space for complementary tests from colliders, DM direct detection and GW interferometers. The spin-independent DM-nucleon cross section in terms of the Higgs portal coupling λ_p is shown for each BP.

shown in Fig. 4, we can see that the future muon collider can probe a portal coupling above the neutrino floor for the xenon experiment, and can fully test the parameter space that predicts a spin-independent DM-nucleon cross section within the future LZ sensitivity. We then obtain an interesting situation for the minimal dark boson world: when the stochastic GW signals are observed by future space-based/terrestrial interferometers, complementary probes via direct detection of a vector DM particle and collider searches for a dark scalar can provide cross-checks for the microscopic origin of GW signals. Nevertheless, the indirect DM signals discussed in Sec. 3.3 are much suppressed. This comes from the fact that $m_{A'} \simeq \mathcal{O}(10)m_\phi$ is generally required when observational GW signals are generated during the dark phase transition. Then, Eq. (3.15) is not satisfied, as can also be seen from Tab. 1 by using Eq. (3.16). Besides, the parameter space shown in Fig. 4 and Tab. 1 indicates that $\lambda_p \ll g_X^2$ and the DM mass is typically at TeV scale, making $(\sigma v)_{A' \rightarrow t}$ estimated in Eq. (3.17) several orders of magnitude smaller than the current bounds [85, 124].

As mentioned in Sec. 2.3, the dark thermalization conditions for the one-temperature treatment of the dark phase transition and DM freeze-out typically require a Higgs portal coupling at $\lambda_p > \mathcal{O}(10^{-6})$. This is shown in Fig. 4, where the purple meshed region denotes a small λ_p that cannot establish a thermal contact between the SM and the dark sectors all the way down to the DM freeze-out temperature $T_{\text{fo}} \simeq m_{A'}/25$. It points out that, for a

Higgs-portal connected minimal dark sector, the interested parameter space for strong GW signals and detectable DM indeed corresponds to a dark boson plasma sharing the same temperature with the SM during the phase transition and the DM freeze-out.

Finally, it is worth mentioning that, while we focus on the one-temperature regime between the SM and dark sectors, the Higgs portal could be too small to establish a common temperature, and the dark sector develops its own temperature with the initial condition dating back to the post-inflationary epoch. However, a much lower dark temperature will dramatically reduce the GW signals, while a higher dark temperature could be favored to boost the GW signals. In the latter case, the entropy injection to the SM plasma from the heavy dark sector would dilute the GW signals after phase transition. The net effect on GW signals was studied in Ref. [125], pointing out that the enhancement effect due a higher dark temperature can dominate in a large region of parameter space. Different from the one-temperature scenario, where λ_p shown in Fig. 4 indicates scalar decay well before the epoch of big-bang nucleosynthesis, indirect detection for a hotter dark sector with a much smaller λ_p could still be feasible in cosmology. Besides, the long-lived scalar could also feature displaced vertices when produced at colliders. Since all these phenomena depend on the parameter set $\{\lambda_p, \lambda, m_\phi\}$, one can expect certain correlation among GW, DM and indirect detection of the long-lived scalar in cosmology and colliders.

7 Conclusion

We have presented a dark boson plasma that can undergo a strong first-order phase transition, generate observable GW signals and provide a DM candidate. The dark gauge boson, as the WIMP-like DM, plays a significant role in triggering the dark phase transition via finite-temperature effects and hence inducing stochastic GW signals. The theoretical framework is so simple and minimal that certain correlations exist in the complementary tests from GW interferometers, direct detection of DM and colliders, all of which serve as promising avenues to help us *hear* and *see* the dark. In particular, we found that the future muon collider in the decay channel $\phi \rightarrow 2h$ is able to probe the full parameter space where GW signals induced from the dark phase transition are detectable by LISA, DECIGO, BBO, AION and AEDGE, and the spin-independent DM-nucleon cross section is reachable by the future LZ experiment above the neutrino floor.

Acknowledgements

We would like to thank Michael J. Ramsey-Musolf, Xun-Jie Xu and Ke-Pan Xie for helpful discussions. S.-P. Li is supported in part by the National Natural Science Foundation of China under grant No. 12141501 and also by CAS Project for Young Scientists in Basic Research (YSBR-099). S. K. is supported in part by JSPS KAKENHI Nos. 20H00160 and 23K17691.

A An analytic perspective of the minimal dark phase transition

An analytic analysis of the dark phase transition allows us to get an efficient overview of the model parameter space where strong GW signals are favored and the connection to DM could become clearer. In this appendix, we discuss the analytic dynamics of the dark phase transition by making some reasonable approximations. We will see that, such an analytic perspective is qualitatively consistent with the numerical analysis performed in the main text.

One of the widely considered potentials that allow analytic treatments [126, 127] has the following polynomial structure [127],

$$V_{\text{poly}}(\varphi, T) = D(T^2 - T_0^2)\varphi^2 - ET\varphi^3 + \frac{\lambda}{4}\varphi^4, \quad (\text{A.1})$$

with field-independent constants D, T_0, E . This polynomial potential is also expected from the minimal dark $U(1)_X$ scenario considered in this work. Explicitly, it can be derived by using the high-temperature expansion of Eq. (4.8) [128, 129],

$$V_T \approx \frac{T^2}{24} \sum_{i=\phi, \chi, A'} n_i m_i^2 - \frac{T}{12\pi} \sum_{i=\phi, \chi, A'} n_i (m_i^2)^{3/2} - \frac{1}{64\pi^2} \sum_{i=\phi, \chi, A'} n_i m_i^4 \ln\left(\frac{m_i^2}{aT^2}\right), \quad (\text{A.2})$$

where $\ln a \approx 5.41$ and we have dropped the φ -independent constants.

The μ -dependence from V_{CW} in Eq. (4.4) can be removed by invoking the RG running of the tree-level parameters in V_0 [130–132], with

$$\lambda(\mu) = \lambda(\mu_0) + \frac{3g_X^4}{16\pi^2} \ln\left(\frac{\mu^2}{\mu_0^2}\right) + \mathcal{O}(\lambda^2), \quad (\text{A.3})$$

$$\mu_S^2(\mu) = \mu_S^2(\mu_0) + \frac{\lambda(\mu_0)}{4\pi^2} \mu_S^2(\mu_0) \ln\left(\frac{\mu^2}{\mu_0^2}\right). \quad (\text{A.4})$$

After applying the daisy resummation (4.10), we finally arrive at the effective potential

$$V_{\text{eff}}(\varphi, T) = \left(\frac{g_X^2}{8}T^2 - \frac{\lambda v_\phi^2}{2}\right)\varphi^2 - \frac{g_X^3 T}{12\pi} \left[2\varphi^3 + \left(\varphi^2 + \frac{T^2}{3}\right)^{3/2}\right] + \frac{\lambda}{4}\varphi^4, \quad (\text{A.5})$$

where only the dominant contribution from the gauge boson is taken into account, and corrections at $\mathcal{O}(\lambda^2)$ and terms proportional to $3g_X^4/(4\pi)^2$ in Eqs. (A.3) and (A.4) are neglected.¹⁶

It can now be seen that, without the daisy resummation in Eq. (A.5), the effective potential reduces to the polynomial form (A.1), with

$$D = \frac{g_X^2}{8}, \quad T_0 = \frac{2\sqrt{\lambda}v_\phi}{g_X}, \quad E = \frac{g_X^2}{4\pi}. \quad (\text{A.6})$$

¹⁶It can also be interpreted by taking λ and μ_S^2 , as well as g_X in Eq. (A.5) evaluated at a fixed RG scale $\mu = \mu_0$.

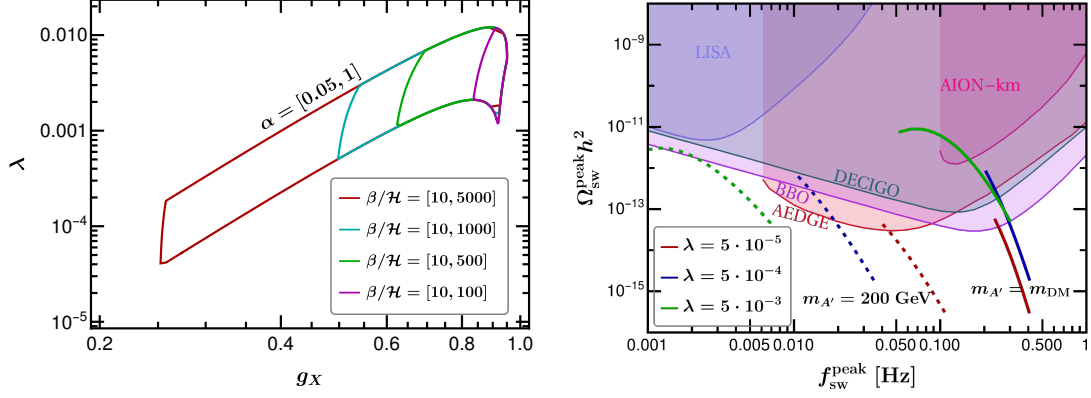


Figure 5. Left: the parameter space in terms of λ and g_X for $0.05 < \alpha < 1$ and for some typical ranges of β/\mathcal{H} . Right: the correlation between the GW peak amplitude $\Omega_{\text{sw}}^{\text{peak}} h^2$ and peak frequency $f_{\text{sw}}^{\text{peak}}$ for some benchmark values of λ under the scan of $0.1 < g_X < 1$. The solid lines are obtained via Eq. (3.13) while the dotted lines are obtained by fixing $m_{A'} = 200$ GeV without assuming a DM candidate.

The potential (A.1) at high temperatures could develop an energy barrier between the false and true vacua. As usual, there is a trivial solution $\varphi = 0$ to $\partial V_{\text{poly}}/\partial\varphi = 0$, corresponding to a local minimum if $4\lambda v_\phi^2 < g_X^2 T^2$. There are two additional solutions to $\partial V_{\text{poly}}/\partial\varphi = 0$, with

$$\varphi_{\pm} = \frac{1}{8\pi\lambda} \left[3g_X^3 T \pm (9g_X^6 T^2 - 16\pi^2 g_X^2 \lambda T^2 + 64\pi^2 \lambda^2 v_\phi^2)^{1/2} \right]. \quad (\text{A.7})$$

To make these extrema physical, we should set

$$64\pi^2 \lambda^2 v_\phi^2 - 16\pi^2 g_X^2 \lambda T^2 + 9g_X^6 T^2 > 0, \quad (\text{A.8})$$

for temperatures T during the phase transition. The local maximum at φ_- is expected to develop an energy barrier between the false vacuum at $\varphi = 0$ and the true vacuum at φ_+ .

The Euclidean action S_3 from the polynomial potential has the following simple analytic solution [133],

$$S_3 \approx \frac{64\pi ET \sqrt{\delta} (\beta_1 \delta + \beta_2 \delta^2 + \beta_3 \delta^3)}{81\lambda^{3/2} (2 - \delta)^2}, \quad (\text{A.9})$$

where $\delta \equiv 2\lambda D(1 - T_0^2/T^2)/E^2$, with D, T_0 and E given in Eq. (A.6), and $\beta_1 = 8.2938, \beta_2 = -5.5330, \beta_3 = 0.8180$. Using this analytic expression, we can evaluate the nucleation temperature via Eq. (4.15), and subsequently the $\alpha, \beta/\mathcal{H}$ parameters.

We show in the left panel of Fig. 5 the parameter space of λ, g_X for $0.05 < \alpha < 1$ and some typical ranges of β/\mathcal{H} . By taking some BP of λ inferred from the left panel, we scan the gauge coupling in the range: $[0.1, 1]$, so as to obtain the relation between $f_{\text{sw}}^{\text{peak}}$ and $\Omega_{\text{sw}}^{\text{peak}} h^2$ from Eqs. (5.2) and (5.3), as shown in the right panel of Fig. 5. Both the short solid and dotted lines are cut by the conditions $0.1 < \alpha < 1, \beta/\mathcal{H} > 1$ and (A.8).

It can be seen that, when A'_μ is the DM candidate, the condition from Eq. (3.13) implies a peak frequency at sub-Hz, with the peak amplitude detectable by AION, AEDGE,

DECIGO and BBO. When relaxing the DM condition, we take a lower mass for the dark gauge boson, $m_{A'} = 200$ GeV, which shifts the peak frequency towards mHz. Note that the LISA sensitivity curve is taken from the analysis given in Ref. [44], rather than the peak-integrated-sensitivity curves from Refs. [112, 113].

B DM annihilation rates

The gauge-scalar interaction is derived from the gauge kinetic term:

$$\mathcal{L}_{\text{kin}} = (\partial_\mu - ig_X A'_\mu)S \cdot (\partial^\mu + ig_X A'^\mu)S^*, \quad (\text{B.1})$$

with $S = (v_\phi + \phi)/\sqrt{2}$ in the unitary gauge. It leads to the Feynman vertices,

$$A'^\mu A'^\nu \phi : 2g_X^2 v_\phi \eta^{\mu\nu}, \quad A'^\mu A'^\nu \phi^2 : 2g_X^2 \eta^{\mu\nu}, \quad (\text{B.2})$$

where $\eta^{\mu\nu}$ is the Minkowski metric. For the dark scalar ϕ , the Feynman vertices from potential (2.1) are given by

$$\phi^3 : -6\lambda v_\phi, \quad \phi^4 : -6\lambda. \quad (\text{B.3})$$

The dark gauge boson freeze-out is dominated by the quartic contact interaction and the t, u -channel annihilation, while the s -channel annihilation carries an additional factor λ^2 and hence is much smaller than the t, u channels for $\lambda \ll g_X^2$. Neglecting the s -channel is a good approximation since there is no s -channel resonant production of ϕ for $m_{A'} \gg m_\phi$. The cross section of $2A'_\mu \rightarrow 2\phi$ can be parameterized as

$$\sigma v \equiv 2(a + bv^2), \quad (\text{B.4})$$

where the factor of 2 takes into account the pair DM annihilation, and v is the relative velocity of incoming DM particles in the lab frame. To determine the cross section, let us now calculate the amplitude of $2A'_\mu \rightarrow 2\phi$, with the Feynman diagrams shown in Fig. 1. The amplitudes in the center-of-mass frame are given by

$$\mathcal{M}_t = \frac{8g_X^4 v_\phi^2 \eta^{\mu\nu} \epsilon_\mu(p_1) \epsilon_\nu(p_2)}{m_\phi^2 - \hat{s}(1 - \beta_{A',\phi} \cos \theta)}, \quad (\text{B.5})$$

$$\mathcal{M}_u = \frac{8g_X^4 v_\phi^2 \eta^{\mu\nu} \epsilon_\mu(p_1) \epsilon_\nu(p_2)}{m_\phi^2 - \hat{s}(1 + \beta_{A',\phi} \cos \theta)}, \quad (\text{B.6})$$

$$\mathcal{M}_c = 2g_X^2 \eta^{\mu\nu} \epsilon_\mu(p_1) \epsilon_\nu(p_2), \quad (\text{B.7})$$

for the t, u channels and contact annihilation, respectively. Here \hat{s} is the Lorentz-invariant Mandelstam variable, $\beta_{A',\phi} \equiv \sqrt{1 - 4m_{A',\phi}^2/\hat{s}}$, and θ is the angle between the momenta of the incoming and outgoing particles in the center-of-mass frame.

The differential cross section in the center-of-mass frame yields

$$\frac{d\sigma}{d\Omega} = \frac{1}{S(2E_1)(2E_2)|\vec{v}_1 - \vec{v}_2|} \left[\frac{1}{16\pi^2} \frac{|\vec{p}_f|}{E_{\text{cm}}} |\mathcal{M}|_{\text{sum}}^2 \right] = \frac{\beta_\phi |\mathcal{M}|_{\text{sum}}^2}{128\pi^2 \beta_{A'} \hat{s}}, \quad (\text{B.8})$$

where $\mathcal{M}_{\text{sum}} = \mathcal{M}_t + \mathcal{M}_u + \mathcal{M}_c$, $1/S = 1/2$ is the symmetry factor accounting for the identical scalar in the final states, and $E_{\text{cm}} = \sqrt{\hat{s}}$. The final-state momentum $|\vec{p}_f|$ in the center-of-mass frame can be expressed in terms of \hat{s} , with $|\vec{p}_f| = \beta_\phi \sqrt{\hat{s}}/2$.

Going to the frame where one of the incoming particles is at rest (the lab frame), as defined in Eq. (B.4), we can parameterize the incoming four-momenta as $p_1 = (E, \vec{p})$, $p_2 = (m_{A'}, 0)$, with the relative velocity $v = |\vec{p}/E|$. Given $E = m_{A'}/\sqrt{1-v^2}$, $|\vec{p}| = m_{A'}v/\sqrt{1-v^2}$, \hat{s} in the lab frame is given by

$$\hat{s} = (p_1 + p_2)^2 = 2m_{A'}^2 \left(1 + \frac{1}{\sqrt{1-v^2}}\right) \approx 4m_{A'}^2 (1 + v^2/4). \quad (\text{B.9})$$

Note that from \hat{s} in the center-of-mass frame we obtain $v^2 = v_{\text{cm}}^2/2$, where v_{cm} is the relative velocity in the center-of-mass frame. It is now straightforward to evaluate the cross section in the lab frame. Expanding the small velocity up to $\mathcal{O}(v^2)$ and neglecting the scalar mass, we obtain the a, b parameters as

$$a \approx \frac{3g_X^4}{16\pi m_{A'}^2}, \quad b \approx -\frac{15g_X^4}{128\pi m_{A'}^2}. \quad (\text{B.10})$$

Based on Eq. (B.4), the collision rate $\gamma_{A'}$ can be written as

$$\gamma_{A'} = \int d\Pi_1 d\Pi_2 d\Pi_3 d\Pi_4 f_1(E_1) f_2(E_2) |\mathcal{M}|_{\text{sum}}^2 (2\pi)^4 \delta^4(p_1 + p_2 - p_3 - p_4) \quad (\text{B.11})$$

$$= \int d\Pi_1 d\Pi_2 f_1(E_1) f_2(E_2) [4\sigma v E_1 E_2] \quad (\text{B.12})$$

$$= 2(a + 6b/x) n_{A'}^2 \quad (\text{B.13})$$

$$\equiv \langle \sigma v \rangle_{A'} n_{A'}^2, \quad (\text{B.14})$$

where $d\Pi_i \equiv d^3p_i / [(2\pi)^3 2E_i]$ is the phase-space factor with E_i the energy, $f_i(E_i)$ is the thermal distribution function of A'_μ with the number density $n_{A'}$, and the quantum statistics for the final states is neglected. Note that in Eq. (B.13), $x \equiv m_{A'}/T$, and the b -dependent term is derived by taking the relative velocity $v^2 = |\vec{p}_1/E_1 - \vec{p}_2/E_2|^2 \approx (p_1^2 + p_2^2 - 2\vec{p}_1 \cdot \vec{p}_2)/m_{A'}^2$ in the phase-space integration with the Boltzmann distribution $f_i(E_i) = e^{-E_i/T}$, without introducing the Møller velocity [79].

References

- [1] P. Schwaller, *Gravitational Waves from a Dark Phase Transition*, *Phys. Rev. Lett.* **115** (2015), no. 18 181101, [[1504.07263](#)].
- [2] M. Pospelov, A. Ritz, and M. B. Voloshin, *Secluded WIMP Dark Matter*, *Phys. Lett. B* **662** (2008) 53–61, [[0711.4866](#)].
- [3] J. L. Feng, H. Tu, and H.-B. Yu, *Thermal Relics in Hidden Sectors*, *JCAP* **10** (2008) 043, [[0808.2318](#)].
- [4] A. Berlin, D. Hooper, and G. Krnjaic, *Thermal Dark Matter From A Highly Decoupled Sector*, *Phys. Rev. D* **94** (2016), no. 9 095019, [[1609.02555](#)].

- [5] J. A. Evans, S. Gori, and J. Shelton, *Looking for the WIMP Next Door*, *JHEP* **02** (2018) 100, [[1712.03974](#)].
- [6] B. Batell, N. Blinov, C. Hearty, and R. McGehee, *Exploring Dark Sector Portals with High Intensity Experiments*, in *Snowmass 2021*, 7, 2022. [2207.06905](#).
- [7] T. Ferber, A. Grohsjean, and F. Kahlhoefer, *Dark Higgs Bosons at Colliders*, [2305.16169](#).
- [8] J. Jaeckel, V. V. Khoze, and M. Spannowsky, *Hearing the signal of dark sectors with gravitational wave detectors*, *Phys. Rev. D* **94** (2016), no. 10 103519, [[1602.03901](#)].
- [9] R. Jinno and M. Takimoto, *Probing a classically conformal B-L model with gravitational waves*, *Phys. Rev. D* **95** (2017), no. 1 015020, [[1604.05035](#)].
- [10] C.-W. Chiang and E. Senaha, *On gauge dependence of gravitational waves from a first-order phase transition in classical scale-invariant $U(1)'$ models*, *Phys. Lett. B* **774** (2017) 489–493, [[1707.06765](#)].
- [11] V. Brdar, A. J. Helmboldt, and J. Kubo, *Gravitational Waves from First-Order Phase Transitions: LIGO as a Window to Unexplored Seesaw Scales*, *JCAP* **02** (2019) 021, [[1810.12306](#)].
- [12] C. Marzo, L. Marzola, and V. Vaskonen, *Phase transition and vacuum stability in the classically conformal B–L model*, *Eur. Phys. J. C* **79** (2019), no. 7 601, [[1811.11169](#)].
- [13] S. Yaser Ayazi and A. Mohamadnejad, *Conformal vector dark matter and strongly first-order electroweak phase transition*, *JHEP* **03** (2019) 181, [[1901.04168](#)].
- [14] A. Mohamadnejad, *Gravitational waves from scale-invariant vector dark matter model: Probing below the neutrino-floor*, *Eur. Phys. J. C* **80** (2020), no. 3 197, [[1907.08899](#)].
- [15] J. Ellis, M. Lewicki, J. M. No, and V. Vaskonen, *Gravitational wave energy budget in strongly supercooled phase transitions*, *JCAP* **06** (2019) 024, [[1903.09642](#)].
- [16] J. Ellis, M. Lewicki, and V. Vaskonen, *Updated predictions for gravitational waves produced in a strongly supercooled phase transition*, *JCAP* **11** (2020) 020, [[2007.15586](#)].
- [17] A. Addazi and A. Marciano, *Gravitational waves from dark first order phase transitions and dark photons*, *Chin. Phys. C* **42** (2018), no. 2 023107, [[1703.03248](#)].
- [18] D. Croon, V. Sanz, and G. White, *Model Discrimination in Gravitational Wave spectra from Dark Phase Transitions*, *JHEP* **08** (2018) 203, [[1806.02332](#)].
- [19] M. Breitbach, J. Kopp, E. Madge, T. Opferkuch, and P. Schwaller, *Dark, Cold, and Noisy: Constraining Secluded Hidden Sectors with Gravitational Waves*, *JCAP* **07** (2019) 007, [[1811.11175](#)].
- [20] T. Hasegawa, N. Okada, and O. Seto, *Gravitational waves from the minimal gauged $U(1)_{B-L}$ model*, *Phys. Rev. D* **99** (2019), no. 9 095039, [[1904.03020](#)].
- [21] J. B. Dent, B. Dutta, S. Ghosh, J. Kumar, and J. Runburg, *Sensitivity to dark sector scales from gravitational wave signatures*, *JHEP* **08** (2022) 300, [[2203.11736](#)].
- [22] S.-P. Li and K.-P. Xie, *Collider test of nano-Hertz gravitational waves from pulsar timing arrays*, *Phys. Rev. D* **108** (2023), no. 5 055018, [[2307.01086](#)].
- [23] I. Baldes, *Gravitational waves from the asymmetric-dark-matter generating phase transition*, *JCAP* **05** (2017) 028, [[1702.02117](#)].

- [24] F. P. Huang and C. S. Li, *Probing the baryogenesis and dark matter relaxed in phase transition by gravitational waves and colliders*, *Phys. Rev. D* **96** (2017), no. 9 095028, [[1709.09691](#)].
- [25] A. Alves, T. Ghosh, H.-K. Guo, K. Sinha, and D. Vagie, *Collider and Gravitational Wave Complementarity in Exploring the Singlet Extension of the Standard Model*, *JHEP* **04** (2019) 052, [[1812.09333](#)].
- [26] I. Baldes and C. Garcia-Cely, *Strong gravitational radiation from a simple dark matter model*, *JHEP* **05** (2019) 190, [[1809.01198](#)].
- [27] L. Bian and Y.-L. Tang, *Thermally modified sterile neutrino portal dark matter and gravitational waves from phase transition: The Freeze-in case*, *JHEP* **12** (2018) 006, [[1810.03172](#)].
- [28] J.-P. Hong, S. Jung, and K.-P. Xie, *Fermi-ball dark matter from a first-order phase transition*, *Phys. Rev. D* **102** (2020), no. 7 075028, [[2008.04430](#)].
- [29] F. Costa, S. Khan, and J. Kim, *A two-component dark matter model and its associated gravitational waves*, *JHEP* **06** (2022) 026, [[2202.13126](#)].
- [30] M. Kierkla, A. Karam, and B. Swiezevska, *Conformal model for gravitational waves and dark matter: a status update*, *JHEP* **03** (2023) 007, [[2210.07075](#)].
- [31] F. Costa, S. Khan, and J. Kim, *A two-component vector WIMP — fermion FIMP dark matter model with an extended seesaw mechanism*, *JHEP* **12** (2022) 165, [[2209.13653](#)].
- [32] Z. Chen, K. Ye, and M. Zhang, *Asymmetric dark matter with a spontaneously broken $U(1)$: Self-interaction and gravitational waves*, *Phys. Rev. D* **107** (2023), no. 9 095027, [[2303.11820](#)].
- [33] G. Arcadi, G. C. Dorsch, J. P. Neto, F. S. Queiroz, and Y. M. Oviedo-Torres, *Probing a Dark Sector with Collider Physics, Direct Detection, and Gravitational Waves*, [2307.06376](#).
- [34] S. R. Coleman and E. J. Weinberg, *Radiative Corrections as the Origin of Spontaneous Symmetry Breaking*, *Phys. Rev. D* **7** (1973) 1888–1910.
- [35] *High-Luminosity Large Hadron Collider (HL-LHC): Technical Design Report V. 0.1*, .
- [36] *Physics and Detectors at CLIC: CLIC Conceptual Design Report*, [1202.5940](#).
- [37] **ILC Collaboration**, *The International Linear Collider Technical Design Report - Volume 2: Physics*, [1306.6352](#).
- [38] J. P. Delahaye, M. Diemmoz, K. Long, B. Mansoulié, N. Pastrone, L. Rivkin, D. Schulte, A. Skrinsky, and A. Wulzer, *Muon Colliders*, [1901.06150](#).
- [39] **LUX Collaboration**, D. S. Akerib *et al.*, *Results from a search for dark matter in the complete LUX exposure*, *Phys. Rev. Lett.* **118** (2017), no. 2 021303, [[1608.07648](#)].
- [40] **XENON Collaboration**, E. Aprile *et al.*, *First Dark Matter Search Results from the XENON1T Experiment*, *Phys. Rev. Lett.* **119** (2017), no. 18 181301, [[1705.06655](#)].
- [41] **PandaX-II Collaboration**, X. Cui *et al.*, *Dark Matter Results From 54-Ton-Day Exposure of PandaX-II Experiment*, *Phys. Rev. Lett.* **119** (2017), no. 18 181302, [[1708.06917](#)].
- [42] **PandaX-4T Collaboration**, Y. Meng *et al.*, *Dark Matter Search Results from the PandaX-4T Commissioning Run*, *Phys. Rev. Lett.* **127** (2021), no. 26 261802, [[2107.13438](#)].

- [43] **LZ Collaboration**, J. Aalbers *et al.*, *First Dark Matter Search Results from the LUX-ZEPLIN (LZ) Experiment*, [2207.03764](#).
- [44] C. Caprini *et al.*, *Detecting gravitational waves from cosmological phase transitions with LISA: an update*, *JCAP* **03** (2020) 024, [[1910.13125](#)].
- [45] C. Cutler and J. Harms, *BBO and the neutron-star-binary subtraction problem*, *Phys. Rev. D* **73** (2006) 042001, [[gr-qc/0511092](#)].
- [46] N. Seto, S. Kawamura, and T. Nakamura, *Possibility of direct measurement of the acceleration of the universe using 0.1-Hz band laser interferometer gravitational wave antenna in space*, *Phys. Rev. Lett.* **87** (2001) 221103, [[astro-ph/0108011](#)].
- [47] L. Badurina *et al.*, *AION: An Atom Interferometer Observatory and Network*, *JCAP* **05** (2020) 011, [[1911.11755](#)].
- [48] **AEDGE Collaboration**, Y. A. El-Neaj *et al.*, *AEDGE: Atomic Experiment for Dark Matter and Gravity Exploration in Space*, *EPJ Quant. Technol.* **7** (2020) 6, [[1908.00802](#)].
- [49] **LZ Collaboration**, D. S. Akerib *et al.*, *LUX-ZEPLIN (LZ) Conceptual Design Report*, [1509.02910](#).
- [50] B. J. Mount *et al.*, *LUX-ZEPLIN (LZ) Technical Design Report*, [1703.09144](#).
- [51] **LZ Collaboration**, D. S. Akerib *et al.*, *Projected WIMP sensitivity of the LUX-ZEPLIN dark matter experiment*, *Phys. Rev. D* **101** (2020), no. 5 052002, [[1802.06039](#)].
- [52] J. Billard, L. Strigari, and E. Figueroa-Feliciano, *Implication of neutrino backgrounds on the reach of next generation dark matter direct detection experiments*, *Phys. Rev. D* **89** (2014), no. 2 023524, [[1307.5458](#)].
- [53] F. Ruppin, J. Billard, E. Figueroa-Feliciano, and L. Strigari, *Complementarity of dark matter detectors in light of the neutrino background*, *Phys. Rev. D* **90** (2014), no. 8 083510, [[1408.3581](#)].
- [54] O. Lebedev, H. M. Lee, and Y. Mambrini, *Vector Higgs-portal dark matter and the invisible Higgs*, *Phys. Lett. B* **707** (2012) 570–576, [[1111.4482](#)].
- [55] Y. Farzan and A. R. Akbarieh, *VDM: A model for Vector Dark Matter*, *JCAP* **10** (2012) 026, [[1207.4272](#)].
- [56] V. Vaskonen, *Electroweak baryogenesis and gravitational waves from a real scalar singlet*, *Phys. Rev. D* **95** (2017), no. 12 123515, [[1611.02073](#)].
- [57] A. Beniwal, M. Lewicki, J. D. Wells, M. White, and A. G. Williams, *Gravitational wave, collider and dark matter signals from a scalar singlet electroweak baryogenesis*, *JHEP* **08** (2017) 108, [[1702.06124](#)].
- [58] K. Hashino, M. Kakizaki, S. Kanemura, P. Ko, and T. Matsui, *Gravitational waves from first order electroweak phase transition in models with the $U(1)_X$ gauge symmetry*, *JHEP* **06** (2018) 088, [[1802.02947](#)].
- [59] A. Denner, S. Heinemeyer, I. Puljak, D. Rebuszi, and M. Spira, *Standard Model Higgs-Boson Branching Ratios with Uncertainties*, *Eur. Phys. J. C* **71** (2011) 1753, [[1107.5909](#)].
- [60] **CMS Collaboration**, A. M. Sirunyan *et al.*, *Search for invisible decays of a Higgs boson produced through vector boson fusion in proton-proton collisions at $\sqrt{s} = 13$ TeV*, *Phys. Lett. B* **793** (2019) 520–551, [[1809.05937](#)].

- [61] J. de Blas *et al.*, *Higgs Boson Studies at Future Particle Colliders*, *JHEP* **01** (2020) 139, [[1905.03764](#)].
- [62] Y. Tan *et al.*, *Search for invisible decays of the Higgs boson produced at the CEPC*, *Chin. Phys. C* **44** (2020), no. 12 123001, [[2001.05912](#)].
- [63] A. Ishikawa, *Search for invisible decays of the Higgs boson at the ILC*, *PoS LeptonPhoton2019* (2019) 147, [[1909.07537](#)].
- [64] K. Fujii *et al.*, *ILC Study Questions for Snowmass 2021*, [[2007.03650](#)].
- [65] C. Potter, A. Steinhebel, J. Brau, A. Pryor, and A. White, *Expected Sensitivity to Invisible Higgs Boson Decays at the ILC with the SiD Detector*, [[2203.08330](#)].
- [66] **CMS Collaboration**, A. M. Sirunyan *et al.*, *Search for a new scalar resonance decaying to a pair of Z bosons in proton-proton collisions at $\sqrt{s} = 13$ TeV*, *JHEP* **06** (2018) 127, [[1804.01939](#)]. [Erratum: *JHEP* 03, 128 (2019)].
- [67] **CMS Collaboration**, A. Tumasyan *et al.*, *Search for a heavy Higgs boson decaying into two lighter Higgs bosons in the $\tau\tau bb$ final state at 13 TeV*, *JHEP* **11** (2021) 057, [[2106.10361](#)].
- [68] **ATLAS Collaboration**, M. Aaboud *et al.*, *Combination of searches for heavy resonances decaying into bosonic and leptonic final states using 36 fb^{-1} of proton-proton collision data at $\sqrt{s} = 13$ TeV with the ATLAS detector*, *Phys. Rev. D* **98** (2018), no. 5 052008, [[1808.02380](#)].
- [69] **ATLAS Collaboration**, G. Aad *et al.*, *Search for heavy diboson resonances in semileptonic final states in pp collisions at $\sqrt{s} = 13$ TeV with the ATLAS detector*, *Eur. Phys. J. C* **80** (2020), no. 12 1165, [[2004.14636](#)].
- [70] **ATLAS Collaboration**, G. Aad *et al.*, *Search for heavy resonances decaying into a pair of Z bosons in the $\ell^+\ell^-\ell'^+\ell'^-$ and $\ell^+\ell^-\nu\bar{\nu}$ final states using 139 fb^{-1} of proton-proton collisions at $\sqrt{s} = 13$ TeV with the ATLAS detector*, *Eur. Phys. J. C* **81** (2021), no. 4 332, [[2009.14791](#)].
- [71] **ATLAS Collaboration**, G. Aad *et al.*, *Search for resonant and non-resonant Higgs boson pair production in the $b\bar{b}\tau^+\tau^-$ decay channel using 13 TeV pp collision data from the ATLAS detector*, *JHEP* **07** (2023) 040, [[2209.10910](#)].
- [72] D. Buttazzo, D. Redigolo, F. Sala, and A. Tesi, *Fusing Vectors into Scalars at High Energy Lepton Colliders*, *JHEP* **11** (2018) 144, [[1807.04743](#)].
- [73] **LHC Higgs Cross Section Working Group Collaboration**, J. R. Andersen *et al.*, *Handbook of LHC Higgs Cross Sections: 3. Higgs Properties*, [[1307.1347](#)].
- [74] **ATLAS Collaboration**, *A detailed map of Higgs boson interactions by the ATLAS experiment ten years after the discovery*, *Nature* **607** (2022), no. 7917 52–59, [[2207.00092](#)]. [Erratum: *Nature* 612, E24 (2022)].
- [75] **CMS Collaboration**, A. Tumasyan *et al.*, *A portrait of the Higgs boson by the CMS experiment ten years after the discovery*, *Nature* **607** (2022), no. 7917 60–68, [[2207.00043](#)].
- [76] R. K. Ellis *et al.*, *Physics Briefing Book: Input for the European Strategy for Particle Physics Update 2020*, [[1910.11775](#)].
- [77] G. C. Branco, P. M. Ferreira, L. Lavoura, M. N. Rebelo, M. Sher, and J. P. Silva, *Theory*

- and phenomenology of two-Higgs-doublet models, *Phys. Rept.* **516** (2012) 1–102, [[1106.0034](#)].
- [78] S. Kanemura, K. Tsumura, K. Yagyu, and H. Yokoya, *Fingerprinting nonminimal Higgs sectors*, *Phys. Rev. D* **90** (2014) 075001, [[1406.3294](#)].
- [79] P. Gondolo and G. Gelmini, *Cosmic abundances of stable particles: Improved analysis*, *Nucl. Phys. B* **360** (1991) 145–179.
- [80] J. M. Cline, K. Kainulainen, and K. A. Olive, *Protecting the primordial baryon asymmetry from erasure by sphalerons*, *Phys. Rev. D* **49** (1994) 6394–6409, [[hep-ph/9401208](#)].
- [81] S. Kanemura, S. Matsumoto, T. Nabeshima, and N. Okada, *Can WIMP Dark Matter overcome the Nightmare Scenario?*, *Phys. Rev. D* **82** (2010) 055026, [[1005.5651](#)].
- [82] S. Baek, P. Ko, W.-I. Park, and E. Senaha, *Higgs Portal Vector Dark Matter : Revisited*, *JHEP* **05** (2013) 036, [[1212.2131](#)].
- [83] E. W. Kolb and M. S. Turner, *The Early Universe*, vol. 69. 1990.
- [84] **Particle Data Group Collaboration**, R. L. Workman *et al.*, *Review of Particle Physics*, *PTEP* **2022** (2022) 083C01.
- [85] **Planck Collaboration**, N. Aghanim *et al.*, *Planck 2018 results. VI. Cosmological parameters*, *Astron. Astrophys.* **641** (2020) A6, [[1807.06209](#)]. [Erratum: *Astron. Astrophys.* 652, C4 (2021)].
- [86] K. Griest and M. Kamionkowski, *Unitarity Limits on the Mass and Radius of Dark Matter Particles*, *Phys. Rev. Lett.* **64** (1990) 615.
- [87] B. W. Lee, C. Quigg, and H. B. Thacker, *Weak Interactions at Very High-Energies: The Role of the Higgs Boson Mass*, *Phys. Rev. D* **16** (1977) 1519.
- [88] **DARWIN Consortium Collaboration**, L. Baudis, *DARWIN: dark matter WIMP search with noble liquids*, *J. Phys. Conf. Ser.* **375** (2012) 012028, [[1201.2402](#)].
- [89] M. Schumann, L. Baudis, L. Büttikofer, A. Kish, and M. Selvi, *Dark matter sensitivity of multi-ton liquid xenon detectors*, *JCAP* **10** (2015) 016, [[1506.08309](#)].
- [90] J. D. Lewin and P. F. Smith, *Review of mathematics, numerical factors, and corrections for dark matter experiments based on elastic nuclear recoil*, *Astropart. Phys.* **6** (1996) 87–112.
- [91] R. J. Hill and M. P. Solon, *Standard Model anatomy of WIMP dark matter direct detection II: QCD analysis and hadronic matrix elements*, *Phys. Rev. D* **91** (2015) 043505, [[1409.8290](#)].
- [92] M. Hoferichter, P. Klos, J. Menéndez, and A. Schwenk, *Improved limits for Higgs-portal dark matter from LHC searches*, *Phys. Rev. Lett.* **119** (2017), no. 18 181803, [[1708.02245](#)].
- [93] A. Sommerfeld, *On the diffraction and deceleration of electrons*, *Annalen Phys.* **403** (1931), no. 3 257–330.
- [94] S. Tulin and H.-B. Yu, *Dark Matter Self-interactions and Small Scale Structure*, *Phys. Rept.* **730** (2018) 1–57, [[1705.02358](#)].
- [95] J. Hisano, S. Matsumoto, M. M. Nojiri, and O. Saito, *Non-perturbative effect on dark matter annihilation and gamma ray signature from galactic center*, *Phys. Rev. D* **71** (2005) 063528, [[hep-ph/0412403](#)].

- [96] N. Arkani-Hamed, D. P. Finkbeiner, T. R. Slatyer, and N. Weiner, *A Theory of Dark Matter*, *Phys. Rev. D* **79** (2009) 015014, [[0810.0713](#)].
- [97] M. Lattanzi and J. I. Silk, *Can the WIMP annihilation boost factor be boosted by the Sommerfeld enhancement?*, *Phys. Rev. D* **79** (2009) 083523, [[0812.0360](#)].
- [98] A. Hryczuk, R. Iengo, and P. Ullio, *Relic densities including Sommerfeld enhancements in the MSSM*, *JHEP* **03** (2011) 069, [[1010.2172](#)].
- [99] J. M. Cline and P.-A. Lemieux, *Electroweak phase transition in two Higgs doublet models*, *Phys. Rev. D* **55** (1997) 3873–3881, [[hep-ph/9609240](#)].
- [100] J. Elias-Miro, J. R. Espinosa, and T. Konstandin, *Taming Infrared Divergences in the Effective Potential*, *JHEP* **08** (2014) 034, [[1406.2652](#)].
- [101] S. P. Martin, *Taming the Goldstone contributions to the effective potential*, *Phys. Rev. D* **90** (2014), no. 1 016013, [[1406.2355](#)].
- [102] J. R. Espinosa, T. Konstandin, and F. Riva, *Strong Electroweak Phase Transitions in the Standard Model with a Singlet*, *Nucl. Phys. B* **854** (2012) 592–630, [[1107.5441](#)].
- [103] P. B. Arnold and O. Espinosa, *The Effective potential and first order phase transitions: Beyond leading-order*, *Phys. Rev. D* **47** (1993) 3546, [[hep-ph/9212235](#)]. [Erratum: *Phys.Rev.D* 50, 6662 (1994)].
- [104] A. D. Linde, *Fate of the False Vacuum at Finite Temperature: Theory and Applications*, *Phys. Lett. B* **100** (1981) 37–40.
- [105] A. D. Linde, *Decay of the False Vacuum at Finite Temperature*, *Nucl. Phys. B* **216** (1983) 421. [Erratum: *Nucl.Phys.B* 223, 544 (1983)].
- [106] C. L. Wainwright, *CosmoTransitions: Computing Cosmological Phase Transition Temperatures and Bubble Profiles with Multiple Fields*, *Comput. Phys. Commun.* **183** (2012) 2006–2013, [[1109.4189](#)].
- [107] M. Hindmarsh, S. J. Huber, K. Rummukainen, and D. J. Weir, *Numerical simulations of acoustically generated gravitational waves at a first order phase transition*, *Phys. Rev. D* **92** (2015), no. 12 123009, [[1504.03291](#)].
- [108] J. R. Espinosa, T. Konstandin, J. M. No, and G. Servant, *Energy Budget of Cosmological First-order Phase Transitions*, *JCAP* **06** (2010) 028, [[1004.4187](#)].
- [109] S. H"ocher, J. Kozaczuk, A. J. Long, J. Turner, and Y. Wang, *Towards an all-orders calculation of the electroweak bubble wall velocity*, *JCAP* **03** (2021) 009, [[2007.10343](#)].
- [110] A. Azatov and M. Vanvlasselaer, *Bubble wall velocity: heavy physics effects*, *JCAP* **01** (2021) 058, [[2010.02590](#)].
- [111] Y. Gouttenoire, R. Jinno, and F. Sala, *Friction pressure on relativistic bubble walls*, *JHEP* **05** (2022) 004, [[2112.07686](#)].
- [112] T. Alanne, T. H"ugle, M. Platscher, and K. Schmitz, *A fresh look at the gravitational-wave signal from cosmological phase transitions*, *JHEP* **03** (2020) 004, [[1909.11356](#)].
- [113] K. Schmitz, *New Sensitivity Curves for Gravitational-Wave Signals from Cosmological Phase Transitions*, *JHEP* **01** (2021) 097, [[2002.04615](#)].
- [114] C. Caprini *et al.*, *Science with the space-based interferometer eLISA. II: Gravitational waves from cosmological phase transitions*, *JCAP* **04** (2016) 001, [[1512.06239](#)].

- [115] C. Caprini, R. Durrer, and G. Servant, *The stochastic gravitational wave background from turbulence and magnetic fields generated by a first-order phase transition*, *JCAP* **12** (2009) 024, [[0909.0622](#)].
- [116] J. Ellis, M. Lewicki, and J. M. No, *On the Maximal Strength of a First-Order Electroweak Phase Transition and its Gravitational Wave Signal*, *JCAP* **04** (2019) 003, [[1809.08242](#)].
- [117] H.-K. Guo, K. Sinha, D. Vagie, and G. White, *Phase Transitions in an Expanding Universe: Stochastic Gravitational Waves in Standard and Non-Standard Histories*, *JCAP* **01** (2021) 001, [[2007.08537](#)].
- [118] J. Ellis, M. Lewicki, and J. M. No, *Gravitational waves from first-order cosmological phase transitions: lifetime of the sound wave source*, *JCAP* **07** (2020) 050, [[2003.07360](#)].
- [119] C. Caprini, D. G. Figueroa, R. Flauger, G. Nardini, M. Peloso, M. Pieroni, A. Ricciardone, and G. Tasinato, *Reconstructing the spectral shape of a stochastic gravitational wave background with LISA*, *JCAP* **11** (2019) 017, [[1906.09244](#)].
- [120] M. Hindmarsh, S. J. Huber, K. Rummukainen, and D. J. Weir, *Shape of the acoustic gravitational wave power spectrum from a first order phase transition*, *Phys. Rev. D* **96** (2017), no. 10 103520, [[1704.05871](#)]. [Erratum: *Phys.Rev.D* 101, 089902 (2020)].
- [121] J. Liu, L. Bian, R.-G. Cai, Z.-K. Guo, and S.-J. Wang, *Primordial black hole production during first-order phase transitions*, *Phys. Rev. D* **105** (2022), no. 2 L021303, [[2106.05637](#)].
- [122] K. Hashino, S. Kanemura, T. Takahashi, and M. Tanaka, *Probing first-order electroweak phase transition via primordial black holes in the effective field theory*, *Phys. Lett. B* **838** (2023) 137688, [[2211.16225](#)].
- [123] **(XENON Collaboration)††, XENON Collaboration**, E. Aprile *et al.*, *First Dark Matter Search with Nuclear Recoils from the XENONnT Experiment*, *Phys. Rev. Lett.* **131** (2023), no. 4 041003, [[2303.14729](#)].
- [124] T. R. Slatyer, *Indirect dark matter signatures in the cosmic dark ages. I. Generalizing the bound on s-wave dark matter annihilation from Planck results*, *Phys. Rev. D* **93** (2016), no. 2 023527, [[1506.03811](#)].
- [125] F. Ertas, F. Kahlhoefer, and C. Tassilo, *Turn up the volume: listening to phase transitions in hot dark sectors*, *JCAP* **02** (2022), no. 02 014, [[2109.06208](#)].
- [126] M. Dine, R. G. Leigh, P. Y. Huet, A. D. Linde, and D. A. Linde, *Towards the theory of the electroweak phase transition*, *Phys. Rev. D* **46** (1992) 550–571, [[hep-ph/9203203](#)].
- [127] M. Quiros, *Finite temperature field theory and phase transitions*, in *ICTP Summer School in High-Energy Physics and Cosmology*, pp. 187–259, 1, 1999. [[hep-ph/9901312](#)].
- [128] L. Dolan and R. Jackiw, *Symmetry Behavior at Finite Temperature*, *Phys. Rev. D* **9** (1974) 3320–3341.
- [129] M. Laine and A. Vuorinen, *Basics of Thermal Field Theory*, vol. 925. Springer, 2016.
- [130] B. M. Kastening, *Renormalization group improvement of the effective potential in massive ϕ^4 theory*, *Phys. Lett. B* **283** (1992) 287–292.
- [131] M. Bando, T. Kugo, N. Maekawa, and H. Nakano, *Improving the effective potential*, *Phys. Lett. B* **301** (1993) 83–89, [[hep-ph/9210228](#)].
- [132] C. Ford, D. R. T. Jones, P. W. Stephenson, and M. B. Einhorn, *The Effective potential and the renormalization group*, *Nucl. Phys. B* **395** (1993) 17–34, [[hep-lat/9210033](#)].

- [133] F. C. Adams, *General solutions for tunneling of scalar fields with quartic potentials*, *Phys. Rev. D* **48** (1993) 2800–2805, [[hep-ph/9302321](#)].